Xia, L.; Storch, H.v.; Feser, F.; Wu, J.:

A study of quasi-millennial extratropical winter cyclone activity over the Southern Hemisphere

In: Climate Dynamics (2015) Springer

DOI: 10.1007/s00382-015-2954-x

A Study of quasi-millennial extratropical winter cyclone activity over the Southern Hemisphere

Lan Xia[1], Hans von Storch[2], Frauke Feser[2], Jian Wu[1]

1 Department of Atmospheric Sciences, Yunnan University, University Town, Chenggong County, Kunming, Yunnan, P. R. China.
2 Institute of Coastal Research, Helmholtz-Zentrum Geesthacht, Geesthacht, Germany.

Abstract

The winter extratropical cyclone activity in the Southern Hemisphere during the last one thousand years within a global climate simulation was analyzed by tracking cyclones, and then clustering them into ten clusters consecutively for each hundred years. There is very strong year-to-year variability for Southern Hemispheric winter extratropical cyclone numbers and larger variations on centennial time scale, more so than for its Northern Hemispherical counterparts. However, no obvious trend can be found. The mean tracks of clusters over the Southern Indian Ocean and near New Zealand shift poleward from the 11th to the 20th century while the clusters in the central Southern Pacific shift equatorward. Storm track clusters with largest deepening rates are found over the Southwestern Indian Ocean. In the 20th century, rapidly deepening cyclones appear more often while long lifespan cyclones appear less frequently. The winter storm activity in the Southern Hemisphere is closely related to the Antarctic Oscillation (AAO). The cyclone frequency over the Indian Ocean and South Pacific Ocean can be associated with the Indian Ocean Dipole (IOD) and El Nino-Southern Oscillation (ENSO) respectively.

1 Introduction

Extratropical cyclones of the Southern Hemisphere (SH) are a dynamically important phenomenon in the mid-latitude climate system, which is not only related to strong winds and heavy precipitation but also influences heat, momentum and moisture fluxes. There are a number of papers that investigated the extratropical cyclone activity over the SH. After first synoptic analyses were prepared by Meinardus and Mecking (1928), a likely first climatology of SH cyclones was provided by Vowinckel and van Loon (1957), and later after the International Geophysical Year 1957/58 by van Loon and Taljaard (1962, 1963). More recent studies dealt with decadal changes of Southern Hemispheric extratropical cyclones using reanalysis data (Key and Chan 1999; Simmonds and Keay 2000ab; Hoskins and Hodges 2005; Wang et al. 2006; Pezza et al. 2007; Lim and Simmonds 2007; Grise et al. 2014), or future changes as an expected response to anthropogenic forcing over the 21st century (Yin 2005; Bengtsson et al. 2006; Chang et al. 2012). However, there is still less knowledge than for the Northern Hemisphere (NH). For example, multi-centennial changes for storminess over the NH are available using proxy data (Alexandersson et al. 1998; Matulla et al. 2008) or global climate model simulations (Fischer-Bruns et al. 2005; Xia et al. 2013), but are still deficient over the SH. So in this paper we examine the storm tracks of the SH for almost 1,000 years within a coupled atmosphere-ocean global climate model (GCM) through the lens of regional clustering and frequency of storm tracks. The purpose of doing so is to learn the long-term natural variability of extratropical cyclones over the SH, which is important for assessing the significance of expected future changes.

This study is making use of an available millennial simulation (J. von Storch et al. 1997). Unfortunately, the spatial resolution of this simulation is only T30 which is relatively coarse and output is saved only every 12 h. It is expected that extratropical cyclone numbers may be underestimated due to coarse temporal and spatial resolution (Zolina and Gulev 2002; Jung et al. 2006). However, the aim of this study is to investigate the variability of SH storm tracks from century to century, and the underestimation of total track lengths and numbers is uniform throughout the simulation so that the variability is supposedly hardly affected. Furthermore, this simulation has been used to study multi-centennial changes for storminess over the NH (Fischer-Bruns et al. 2005; Xia et al. 2013). More important is that the spatial patterns and relative frequencies of tracks are comparable with other studies.

Automatic tracking algorithms provide convenient ways to study long-term cyclone activities (Murray and Simmonds 1991; Hodges 1994, 1995; Serreze 1995; Blender et al. 1997; Wernli and Schwierz 2006; Rudeva and Gulev 2007; Zahn and von Storch 2008ab; Chen et al. 2014). The well-developed tracking algorithm from Hodges (1994, 1995, and 1999) is applied in this study. This algorithm has been already adopted to track SH extratropical cyclones (Hoskins and Hodges 2005; Grise et al. 2014). Also the cluster analysis is commonly used to sort cyclones into different categories (Blender et al. 1997; Sickmöller et al. 2000; Elsner 2003; Nakamura et al. 2009; Chu et al. 2010; Xia et al. 2013).

SH extratropical cyclone activity can be related to many climate factors, for example to the influence of the Antarctic sea ice concentration or extent (Simmonds and Wu 1993; Pezza et al. 2008), also to the effect of the Antarctic Oscillation (AAO) (Fischer-Bruns et al. 2005; Mendes et al. 2010; Eichler and Gottschalck 2013), to the El Nino-Southern Oscillation (ENSO) and Southern Annular Mode (SAM) (Pezza et al. 2008), Indian Ocean Dipole (IOD) (Ashok et al. 2007), as well as to anthropogenic forcing like increases of greenhouse gases (Yin 2005; Bengtsson et al. 2006; Chang et al. 2012) and depletion of Antarctic stratospheric ozone (Grise et al. 2014).

In this paper, variability of SH extratropical cyclones and its relation to southern winter circulation patterns are studied, which is done by aligning seasonal anomalies of mean sea level pressure field (MSLP) and time-variable numbers of members in cyclone track clusters through a Canonical Correlation Analysis (CCA) (Busuioc and von Storch 1996; von Storch and Zwiers 1999).

The long-term simulation dataset generated by the coupled atmosphere-ocean GCM ECHO-G exposed to estimated forcings of solar variations, volcanic and greenhouse-gases in the last millennium, is described in Section 2, as well as the main methods used in this study. In Section 3.1 the time series of SH extratropical cyclone track numbers for the quasi-millennium (991 years) and for each century are shown. In section 3.2 SH cyclone tracks are clustered into ten clusters by the K-means clustering method; characteristics including life span, frequency and intensity for each group are also discussed. Relations between winter circulation patterns and variations of the numbers of the clusters in the South Pacific, South Atlantic and South Indian Ocean are studied in Section 3.3. Finally, the main conclusions are summarized.

2 Data and methods

2.1 Data

The quasi-millennial (1000–1990 AD) simulation used in this study has been carried out with the global climate model ECHO-G (Min et al. 2005 a, b) which consists of the atmospheric model ECHAM4 (Roeckner et al. 1996) and the ocean model HOPE-G (Wolff et al. 1997). There are 19 (20) levels for the atmosphere (ocean). The horizontal resolution is T30 (about 3.75°) for the atmospheric part and T42 (about 2.8°) for the oceanic part. The model time step for ECHAM4 is 30 min and for HOPE-G is 12h. The output is stored every 12 hours.

The estimated historical forcing for driving the model such as solar variations, CO_2 and CH_4 concentrations as well as volcanic effects have been described previously by von Storch et al. (2004) and Zorita et al. (2005). The ECHO-G simulations have been shown to describe well most aspects of the seasonal and annual climatology and of the interannual to decadal variability of near-surface temperature, precipitation and mean sea level pressure (MSLP) (Min et al. 2005 a, b; Gouirand et al. 2007). However, there are weak negative pressure biases at SH mid-latitudes and a strong positive pressure bias over Antarctica which may be related to a lack of ozone depletion in the model (Min et al. 2005a). The atmospheric circulation of the SH including the El Niño Southern Oscillation (ENSO) (Min et al. 2005b), the Antarctic Circumpolar Wave (Marsland et al. 2003) and decadal modulations of ENSO (Rodgers et al. 2004) are also simulated realistically by ECHO-G, although the modeled signal of the ENSO is too large and its frequency is too regular (Min et al. 2005b).

Investigations of shorter simulations done with ECHO-G have already shown that the grid resolution of T30 is sufficient to study mid-latitude baroclinic cyclones (Stendel and Roeckner 1998, Raible and Blender 2004, Fischer-Bruns et al. 2005). The storm tracks were found to agree well with ERA-15/ECMWF reanalysis data and deviations from ERA-15 are below 10% (Stendel and Roeckner, 1998). It can be speculated that simulations carried out on higher spatially resolved grids could lead to an increase in the numbers of cyclones due to the generation of additional smaller and weaker cyclones. With respect to the development of temperature, comparisons with different proxy reconstructions have been done, including tree ring data and borehole temperatures (González-Rouco et al. 2003, Tan et al. 2009), and limited observational data (Min et al. 2005a). These results indicate that this simulation lies within the envelope of reconstructions of the past temperature evolution and exhibits qualitatively similar characteristics with other simulations extending over 1000 and more years. Some have argued that ECHO-G temperature variations would be too large. However, this does not question our main conclusion, namely that the mid-latitude winter storm activity is remarkably stationary on centennial time scales.

The key added value of this simulation is the homogeneous presentation of a possible development during the last millennium which is hardly available for observational data.

2.2 Cyclone tracking and clustering

A well-developed tracking algorithm by Hodges (1994, 1995 and 1999) is applied for cyclone identification and tracking. This algorithm has been widely used to study climatologies of extratropical cyclones (Hoskins and Hodges 2002, 2005; Xia et al. 2013), tropical storms and monsoon depressions (Hodges 1999), or specific cyclones such as polar lows (Xia et al. 2012). It was also adopted to explore SH storm tracks (Hoskins and Hodges 2005).

In this study, the tracking is done with mean sea level pressure (MSLP) fields of the ECHO-G simulation and only winter cyclones (JJA) at mid-latitudes (⩾30° S) in the SH are considered. Before tracking, contributions from zonal wavenumbers less than or equal to 5 are subtracted to remove large-scale features (Hoskins and Hodges 2002). Then the tracking algorithm determines all minima below -1 hPa in the filtered MSLP fields. Minima are connected to form tracks if their distance is less than 12° (about 1,333 km) within 12 h. Minimum lifetimes of tracks are set to 2 days.

No temporal interpolation of the 12-hourly MSLP fields is done for generating shorter time steps (as in e.g. Murray and Simmonds 1991; Zolina and Gulev 2002). To get smooth tracks, B-spline interpolation (Dierckx 1981, 1984) is used to overcome the coarseness of the T30 resolution (Hodges 1994, 1995) and a smoothing procedure with cost function is also applied as suggested by Hodges (1994, 1995 and 1999).

For each century, all tracks are clustered into ten groups by the K-means method which is widely used for the cluster analysis (Blender et al. 1997; Elsner 2003; Mendes et al. 2010; Nakamura et al. 2009). Before clustering, each track is fitted to a second-order polynomial function with six free parameters as suggested by Chu et al. (2010). More technical details about clustering are described by Xia et al. (2013).

3 Results

3.1 Storm tracks

Densities of genesis describe the regions of formation of storm tracks (Fig.1). The genesis maximum is located in the north of New Zealand and as well as in the Tasman Sea near Australia. There are also genesis maxima off Victoria Land and over the south of South Africa which are in accordance with Hoskins and Hodges (2005) and Simmonds and Keay (2000b). Other genesis regions can be found in the western and central Indian Ocean, and across the Atlantic and Pacific Oceans. The pattern of genesis areas agrees quite well with the result of Hoskins and Hodges (2005) who used vorticity from the ERA-40 with the same tracking method and the pattern is also comparable with the one of Simmonds and Keay (2000b) who used NCEP-NCAR reanalysis. In general it can be concluded that the midlatitude cyclone statistics of the SH from the ECHO-G simulation data are realistic.

The 991-year time series of winter (JJA) cyclone numbers for the SH (Fig. 2a) reveal a very strong year-to-year variability. 50-year running means for the whole time series are also shown (Fig. 2b). We can see there are no obvious trend for cyclone numbers and no corresponding relations between cyclone numbers and temperature variations (Fig. 2). Average centennial cyclone numbers (Fig. 3 black line) are at their minimum in the 11^{th} century (1001-1100) with 175.4/year.

The highest average cyclone number of 179.3/year occurs in the 15th century (1401-1500). For the other centuries the average is around 177-178/year. Generally, the variability of average cyclone numbers for different centuries is quite small. No long-term trends can be found during the winters of years 1000-1990.

The result is consistent with the result of Fischer-Bruns et al. (2005) who used the storm frequency defined by the maximum wind speed based on the ECHO-G simulation. A comparison with the storm frequency for both hemispheres between the pre-industrial period (1551-1850) and the industrial period (1851-1990) reveals negligible differences. No noticeable difference can be seen by comparing 1851-1990 with the recent period 1961-1990 as well as for severe storm days. Fischer-Bruns et al. (2005) also divided the 1000-year time series of maximum 10m wind speed into 300 years intervals and found that storm activity is remarkably stable with little variability from period to period.

Our result is also very similar to that obtained for the NH (Xia et al. 2013) when the same tracking method was applied to the ECHO-G simulation. It seems that the average centennial SH cyclone numbers are more closely related to temperature variations than over the NH (refer to Fig. 4 of Xia et al. 2013), even if anomalous temperature periods such as the Medieval Warm Period or the Little Ice Age are hardly associated with strong anomalies in cyclone numbers. Again, average cyclone numbers for different centuries vary only little.

3.2 Clustering results

All tracks for each century are clustered into ten groups by applying the K-means method. Fig. 4 shows the ten clusters of tracks in the 20th century (years 1901-1990). The centroid track is the mean track of each cluster (Fig. 4: red tracks). We can see that the trajectories of the 10 clusters almost make a full circle in the mid-latitudes of the SH and are consistent with the genesis areas (Fig. 1). Over the Indian Ocean, there are four clusters: cluster 1 from New Zealand to Australia, cluster 2 from the southeast of Australia to 90°E, cluster 3 from 90°E to 60°E, cluster 4 from 60°E to South Africa. Over the South Atlantic Ocean, tracks are clustered into two groups: cluster 5 in the western South Atlantic Ocean, cluster 6 in the eastern South Atlantic Ocean. Over the South

Pacific Ocean, tracks are separated into four clusters: cluster 7 from South America to about 90°W, cluster 8 from about 90°W to 120°W, the center of cluster 9 from about 130°W to 170°W, cluster 10 from 170°W to New Zealand. The centroid tracks of the SH bend poleward at their origins while those on the NH bend poleward at their ends (Fig. 5 of Xia et al. 2013).

Table 1 gives the numbers of tracks for each cluster from 1000 to 1990. Cluster 6 which extends from 10°W to South America has the highest numbers. Cluster 9 in the South Pacific Ocean has the fewest numbers. In the Indian Ocean, cluster 1 has the most tracks while cluster 3 has the fewest. Over the South Atlantic, cluster 6 is larger than cluster 5. In the South Pacific Ocean, cluster 7 is the largest, while cluster 9 is the smallest. The sum of cyclone tracks over the South Pacific Ocean (cluster 7, 8, 9 and 10) is higher than that over the Indian Ocean (cluster 1, 2, 3 and 4). And over the South Atlantic Ocean, the sum of cyclone counts (cluster 5 and 6) is the lowest.

Many studies implied that under man-made climate change storm tracks would shift poleward in the SH (Ulbrich and Christoph 1999; Fischer-Bruns et al. 2005; Bengtsson et al. 2006, 2009). This claim is also supported by satellite data showing that recent extratropical storm cloudiness has shifted polewards (Bender et al. 2012). Here, we consider the movement of the track centroids of our ten clusters from the first century (the 11^{th} century) to the last century (the 20^{th} century) (Fig.5). Cluster 1, 2, 3 over the Indian Ocean and cluster 10 over the South Pacific move indeed poleward. However, Cluster 9 moves equatorward and cluster 8 also shifts a little equatorward. The poleward-shifting group (cluster 1, 2, 3, and 10) shifts eastward. Cluster 5, 7 and 8 shift westward. The equatorward shift of cluster 9 and poleward shift of cluster 10 is significant (with 95% confidence; $p < 0.01$), as well as the eastward migration of cluster 1 (with 95% confidence; $p < 0.05$).

Bengtsson et al. (2006) suggested that a poleward movement of the maximum zonal SST gradient is a contributing factor in the poleward shift of the storm track in the SH. In the meantime, many studies showed that the Southern Annular Mode (SAM) (also referred to as Antarctic Oscillation (AAO)), which is the primary pattern of climate variability in the SH, associates with the location and intensity of the polar jet stream and influences cyclone activity of the SH (Fischer-Bruns et al.

2005; Mendes et al. 2010; also see section 3.3). The positive phase of the SAM enhances the pressure gradient between Antarctica and midlatitude and leads to a strengthening and poleward migration of the SH storm tracks and jet streams, similarly to what is observed during a contraction of the sea ice (Pezza et al. 2008). Abram et al. (2014) pointed out that SAM shifts the positive phase since the 15th century and the long-term mean SAM index is now at its highest level that could interpret the poleward shifts of the storm tracks over the Indian Ocean and South Pacific. Furthermore, the study of Graff and Lacasce (2012) supports the notion that the storm tracks respond to changes in both the mean SST and SST gradients: increasing the mean SST and increasing the mid-latitude SST gradient are associated with an intensification and a poleward shift of the storm tracks while a steepening tropical SST gradient causes an equatorward shift of storm tracks. Like, El Nino (La Nina), which is a warming (cooling) of the ocean surface in the tropical eastern Pacific, coupled with the negative (positive) phase of SAM causes the Pacific storm track to shift equatorward (poleward). This happened in the Medieval Climate Anomaly transition to the Little Ice Age (Medieval Climate Anomaly) (Abram et al. 2014; Goodwin et al. 2014). Pezza et al. (2007) suggested that cyclone latitudinal shifts are also related to the Pacific Decadal Oscillation (PDO) phase, i.e. there are more cyclones in the equatorial western Pacific and Indian Ocean during the PDO positive phase while more cyclones occur in subtropical areas during the PDO negative phase.

Figure 6 shows the average cyclone numbers for the 10 clusters in different centuries. There are differences of average cyclone numbers between different clusters, while for most clusters there is no large variation between different centuries. New studies support that the Medieval Warm Period and Little Ice Age are of global scope and not limited to the NH (Rosenthal et al. 2013; Chambers et al. 2014). Neukom et al. (2014) used a new millennial ensemble reconstruction of annual temperature variation for the SH and supported that there is a global cold phase coinciding with the peak of the Northern Hemisphere “Little Ice Age”. For clusters 2, 3, and 4 there are slight increases of average cyclone numbers in the 17th century, but for clusters 7 and 10 there are small declines. Still, there are no systematic changes of cyclone numbers during these temperature anomalies periods. It is also notable that cyclone numbers of cluster 9 and 10 increase markedly in the 20th century. This is consistent with the results of Simmonds and Keay (2000a) based on

1958-97 NCEP data, which show positive linear trends of the annual average cyclone system density around Australia, over the Tasman Sea and in the east of New Zealand. Wang et al. (2004) showed similar results.

Table 2 shows the distribution of lifetimes for all clusters. For clusters 1 to 8, over 30% of all cyclones last 2 to 4 days (Fig. 7). Cluster 9 has the highest percentage (42.56%) of cyclones which last 2 to 4 days. And cluster 10 has the fewest cyclones (27.88%) which last 2 to 4 days but the cluster has the most cyclones (13.75%) which last over 10 days (Fig. 7c). Compared to Northern Hemispheric mid-latitude cyclones (Table 2 of Xia et al. 2013), it can be found that the mid-latitude cyclones of the SH have higher percentages of cyclones which last over 10 days. This is likely related to characteristics of land-sea distribution in the SH which is favorable for the development of cyclones and for sustainability because of the availability of heat and moisture over the large ocean. Cluster 1 contains the highest percentage (11.57%, relative to all its cyclones) of long-lived cyclones (≥ 10 days) over the Indian Ocean (Table 2: numbers in brackets). Over the South Atlantic, the number of long-lived cyclones of cluster 6 (12.25%) is larger than that of cluster 5 (7.39%). For the South Pacific, cluster 10 has the highest percentage (16.64%) of cyclones lasting more than 10 days.

Deepening rates present intensity changes of cyclones during their lifetime. Frequency distributions of deepening rates for all clusters were studied. The mean deepening rate is calculated along the track from genesis location to the maximum pressure value and the maximum deepening rate is the largest pressure fall during this part of the track. The mean deepening rates per 12 h of the ten clusters for the whole time period (year 1000-1990) are listed in Table 3 and normalized ones across different clusters are given in brackets. In contrast to the cyclones of the NH which are more differentiated (Table 4 of Xia et al. 2013), the distributions of the mean deepening rates are quite uniform and similar for all clusters in the SH. The highest percentages for average deepening rates are between 2 to 4 hPa/12 h for all clusters (Table 3 and Fig. 8). The percentage of the average deepening rates over 10 hPa/12 h is the lowest for all clusters.

Table 4 and Fig. 9 give the distributions of maximum deepening rates per 12 h. The highest percentages of maximum deepening rates fall between 4 to 6 hPa/12 h for all clusters (Table 4 and Fig. 9). Over the Indian Ocean, cluster 3 has the highest maximum deepening rate (13.66%) of more than 10 hPa/12 h (Table 4: numbers in brackets). Also, cyclones deepening rapidly (over 10 hPa/12 h) are found mostly over the western Indian Ocean in clusters 3 and 4 (Table 4). In the South Atlantic, cluster 6 of a rapid maximum deepening rate of more than 10 hPa/12 h (14.91%) is larger than cluster 5 (10.92%). For the South Pacific, cluster 7 contains the most cyclones (10.97%) with a rapid maximum deepening rate of more than 10 hPa/12 h. Generally, maximum deepening rates of more than 10 hPa per 12h occur more often over the Indian Ocean (38.66%) than over the South Pacific (35.51%). Over the South Atlantic cyclones with rapid maximum deepening rates over 10 hPa/12 h (25.83%) are the least. However, the maximum deepening rates over 10 hPa/12 h in the Atlantic (clusters 5 and 6) and Pacific (clusters 7, 8, 9 and10) of the SH (Table 4) are smaller than the counterparts of the NH (Table 4 of Xia et al. 2013: clusters 4, 5 and 6 for the Pacific, clusters 8, 9 and 10 for the Atlantic).

The changes of the maximum deepening rates for the Indian Ocean, the South Atlantic, and the Pacific during different centuries were also considered. Here, only the results of typical clusters over three basins are shown (Fig. 10). For instance, for cluster 1, maximum deepening rates larger than 10 hPa per 12 h became more frequent in the 11^{th}, 14^{th} and 20^{th} century, but less frequent in the 12^{th} , 17^{th} and 18^{th} century. For cluster 1 in the 20^{th} century the maximum deepening rates of 0-4 hPa per 12 h and larger than 8 hPa per 12 h became more frequent, but those of 4-6 hPa per 12 h became less frequent. For cluster 6 over the South Atlantic, the maximum deepening rates of 2-4 hPa per 12 h decrease while those larger than 10 hPa per 12 h increase in the 20^{th} century. For cluster 10 relatively slowly deepening cyclones (0-4 hPa/12 h) appear more often in the 20^{th} century, however those deepening relatively fast (>4 hPa/12 h) appear less often (Fig. 10). It is very important to notice that in the 20^{th} century all clusters except for cluster 10 show increasing frequencies of rapidly deepening cyclones (over 10 hPa/12 h) although some clusters are not significant (not shown).

Figure 11 gives the changes of lifetime distributions during different centuries for cluster 1 (over the Indian Ocean), cluster 6 (over the South Atlantic) and cluster 10 (over the South Pacific).

Cyclones lasting longer than 10 days are more frequent in the 11th and 14th century for clusters 1 (Fig. 11). In the South Atlantic, the frequencies of cyclones with long lifespan (over 10 days) increase notably in the 14th century for cluster 5 and in the 18th century for cluster 6. It is found that in the 20th century there are tendencies of decreases in the frequency of long lifespan cyclones (over 10 days) for most clusters and these are significant for clusters 1, 6 and 10 (Fig. 11). However, it is noteworthy that in the 20th century there are significant increases in the frequency of long lifespan cyclones (≥ 8 days) for cluster 9 in the South Pacific.

3.3 Links to large-scale pressure patterns

Storm activity in the SH is strongly related to climate variability. In this study, we investigate how seasonal (JJA) mean MSLP patterns are associated with the annual variability of winter cyclone numbers using the Canonical Correlation Analysis (CCA) (von Storch and Zwiers 1999). The systematic association of winter MSLP fields and winter cyclone numbers are determined separately of the clusters over the Indian Ocean, the South Atlantic and Pacific. In preparation for the CCA, the high-dimensional MSLP fields are truncated to the first thirteen Empirical Orthogonal Functions (EOFs) (von Storch and Zwiers 1999). All analyses are based on anomalies of the quasi-millennium (year 1000 to 1990) mean.

Figure 16 and 17 give the two most important related patterns linking MSLP and cyclone number anomalies in the *Indian Ocean*. The coefficient time series of the first (second) CCA pattern have a correlation of 0.42 (0.33) and the pattern describes 25 % (25 %) of the variance of winter cyclone numbers over the Indian Ocean.

In the first Indian Ocean pattern (Fig. 16) negative pressures anomalies over Antarctica and the vicinity go along with positive pressure anomalies at mid-latitudes. When the CCA time coefficient of the cyclone count is 1, Antarctica and mid-latitudes with a pressure contrast of about 4 hPa, then the number of cyclones in cluster 1 increases by 0.45, in cluster 2 by 3.41 and in cluster 3 by 0.25, but decreases by -1.14 in cluster 4. Thus, when the CCA pattern has a positive coefficient, cyclone numbers in the eastern and middle Indian Ocean (clusters 1, 2 and 3) increase whereas cyclone counts in the western Indian Ocean (cluster 4) decrease. This pattern seems to be related to the Antarctic Oscillation (AAO) which is associated with the location and intensity of the polar jet stream and influences cyclone activity of the SH (Fischer-Bruns et al. 2005; Mendes et al. 2010).

The second Indian Ocean pattern (Fig. 17) describes negative pressure anomaly centers located in the southwest of Australia and in the high-latitudes of the South Pacific while large positive pressure anomaly areas propagate from the South Atlantic to the South Pacific. This relates to the strong increase of cyclone numbers in the eastern Indian Ocean (cluster 1) but decreases in the middle and western Indian Ocean (clusters 2, 3 and 4). According to Ashok et al. (2007), the Indian Ocean Dipole (IOD) phenomenon can remotely influence winter storm track activity over the SH mid-latitude regions. It seems that this pattern is linked to a negative IOD event with increases of storm track activity over South Australia and portions of New Zealand (cluster 1). This is consistent with the results of Ashok et al. (2007) that during a positive (negative) IOD event, the westerlies and storm track activity weaken (enhance) and therefore lead to a significant deficit (surplus) in winter precipitation over the Australia-New Zealand region.

Figures 18 and 19 are the first and second CCA patterns for clusters 5 and 6 over the *South Atlantic*. The first pattern has a correlation of only 0.33 for the coefficient time series and the second pattern shares a correlation of 0.29. They present about 42 and 58 %, respectively, of the variance of year-to-year winter cyclone numbers.

The first South Atlantic pattern (Fig. 18) goes with large negative anomalies around the high latitudes of the SH and positive anomalies over the mid-latitude areas which is related to the positive AAO. When the CCA time coefficient of cyclone count is 1, the cyclone numbers in the South Atlantic increase by 1.91 for the eastern cluster 5 and 2.91 for the western cluster 6. This agrees with Mendes et al. (2010) that AAO could influence the cyclone density of the South American-Southern ocean sector. The second South Atlantic pattern (Fig. 19) has large positive values over the high latitudes while negative values occur over the South Atlantic and parts of the Pacific. It relates to a decrease of cyclone numbers for cluster 5 by -3.14, but an increase for cluster 6 by 2.58.

Figure 20 is the first CCA pattern for clusters 7, 8, 9 and 10 over the *South Pacific*. It presents 31% of the variance for the year-to-year winter cyclone numbers of the Southern Pacific and has a correlation of 0.44 for the coefficient time series. It shows a pattern with positive MSLP anomalies located in the South of Australia and over the Bellingshausen Sea while negative anomalies prevail over the central South Pacific. This pattern is related to increases of cyclone numbers over the eastern South Pacific (by 2.70 for cluster 7 and 2.17 for cluster 8), but decreases of cyclone numbers over the western South Pacific (by -0.55 for cluster 9 and -2.64 for cluster 10). It can be seen that the pattern seems to be related to the central Pacific El Nino-like pattern which is very similar to the results presented by Goodwin et al. (2014: Fig. 1b).

Figure 21 is the second CCA pattern over the *South Pacific*. This pattern has a correlation of 0.42 for the coefficient time series and presents 19% of the variance for the year-to-year winter cyclone numbers of the Southern Pacific. We can see that there are positive pressure anomalies over the eastern South Pacific, but negative anomalies over the western South Pacific. This may be related to the cool phase of ENSO (i.e. La Niña) and there are higher cyclone numbers over the South Pacific especially for cluster 8 (by 2.01) and cluster 10 (by 2.76). It is also worthy to note that the Pacific Decadal Oscillation (PDO), which is related to AAO and ENSO, could influence the SH cyclone activities including numbers, latitudinal position and intensity. For example, Pezza et al. (2007) found that El Nino (La Nina) type condition usually occurs during the positive (negative) phase of the PDO. And the negative phase of the PDO is associated with more but less intense cyclones while the positive phase of the PDO is associated with fewer but more intense cyclones for the mid-high latitudes (Pezza et al. 2007).

4 Conclusions and discussions

A global climate model (ECHO-G) simulation for approximately the last one thousand years was used to investigate the changes of winter extratropical cyclone activity for the SH. The ECHO-G model was driven by the historical forcing of realistic variations of shortwave solar input, time-dependent presence of volcanic material in the upper atmosphere, and slowly changing greenhouse gas concentrations during the last millennium (years 1000-1990). A tracking algorithm developed by K. I. Hodges (1994, 1995 and 1999) was applied to track extratropical cyclones within the simulated MSLP fields. The main result of this study is that the time series of the SH cyclone counts for years 1000 to 1990 show strong year-to-year variations, but no obvious trend. The centennial variability of storm tracks is small. This result is quite similar to the one for the NH found before with the same ECHO-G simulation (Xia et al. 2013).

Cyclone tracks are clustered into ten groups using the K-means method. There are four clusters over the Indian Ocean, two clusters over the South Atlantic and four clusters over the South Pacific. Cyclone numbers of the South Pacific are the highest while the lowest ones are over the South Atlantic. The mean track positions of each cluster are also compared between the first century (the 11th century) and the last century (the 20th century). In the 20th century, the track positions over the Indian Ocean (clusters 1, 2, and 3) and near New Zealand (cluster 10) shift poleward while cluster 9 over the South Pacific shifts equatorward. This is quite different from Northern Hemispheric cyclone positions which change only marginally (Xia et al. 2013). There are small variations on centennial time scales for most clusters. It should be noticed that cyclone numbers in clusters 9 and 10 over the eastern Pacific increase clearly in the 20th century.

Compared to the Northern Hemispheric mid-latitude cyclones (Xia et al. 2013), the Southern Hemispherical cyclones have higher percentage of long lifespan (last over 10 days). In the 20th century frequencies of cyclones lasting more than 10 days decrease for most clusters except for clusters 4 and 9. The highest percentage of average deepening rates for the Southern Hemispherical cyclones is between 2 to 4 hPa/12 h for all clusters. The percentage of maximum deepening rates over 10 hPa/12 h over the oceans of the SH are smaller than the oceanic counterparts of the NH. It is noteworthy that in the 20th century frequencies of rapidly deepening cyclones (maximum deepening rates over 10 hPa/12 h) increase for all clusters of the SH except for cluster 10.

Fischer-Bruns et al. (2005) pointed out that the storm activity in the SH is closely related to the Antarctic Oscillation (AAO) and the pattern of AAO elongates with the CO_2 increase. In our study, the positive AAO pattern is correlated with increased cyclone frequency in the eastern Indian

Ocean, the South Atlantic and the eastern South Pacific which agrees with Mendes et al. (2010) and Eichler and Gottschalck (2013). The study of Fischer-Bruns et al. (2005) also shows that the AAO index is highly associated with the storm shift index. Abram et al. (2014) found that the long-term mean of the SAM (AAO) index is now at the highest positive value for the past 1,000 years which results in a poleward shift of the regions with high storm frequency for the SH. Besides, cyclone frequency over the Indian Ocean and the South Pacific are connected with the Indian Ocean Dipole (IOD) and ENSO. El Nino (La Nina) events associated with negative (positive) SAM states influence storm tracks and westerlies which are confirmed by instrumental studies (Abram et al. 2014 and Goodwin et al. 2014).

There are a number of caveats of this study: First, the external forcing of ECHO-G may deviate from reality and the solar and volcanic forcing may be overestimated. But, even with larger variations of temperature, the centennial variations of SH storm track statistics are still small. Thus, the main conclusions will not be affected. However, Neukon et al. (2014) pointed out that climate models would overestimate the strength of external forcing but underestimate the role of internal ocean-atmosphere dynamics particularly in the SH, and tend to overemphasize Northern Hemisphere-Southern Hemisphere synchronicity. This may explain the similarity on variations of cyclones between the NH (Xia et al. 2013) and SH based on the same ECHO-G simulation. And the deficiencies of the model lead to uncertainties in estimating and attributing cyclone variations. Secondly, there may be underestimations of cyclone tracks due to the coarse spatial resolution (T30) and relatively infrequent storing (every 12 h) of MSLP fields. This may lead to a reduced variability of storm activity. However, we argue that this would be stationary in time, so that the temporal variability would not be affected. Thirdly, this study is a result of just one single model. Their significance will be shown with other similar millennial simulations with better spatial and temporal resolution in the future. But all in all, these caveats must be addressed.

Acknowledgments

We thank Eduardo Zorita for providing the ECHO-G simulation data, his support with statistic routines, and helpful discussions. We appreciate Kevin I. Hodges' help with his tracking algorithm which was used for our study. We also acknowledge the German Climate Computer Center

(DKRZ) Hamburg for the provision of high performance computing platforms. This study is sponsored by Yunnan Applied Basic Research Project (Foundation No. 2014FD003). The authors appreciate two anonymous reviewers for their constructive and helpful comments and suggestions.

References

Abram N. J., R. Mulvaney, F. Vimeux, S. J. Phipps and et al., 2014: Evolution of the Southern Annular Mode during the past millennium. *Nature Climate Change*, **4**, 564-569.

Alexandersson H., T. Schmith, K. Iden, and H. Tuomenvirta, 1998: Longterm variations of the storm climate over NW Europe. *Global Atmosphere and Ocean System.*, **6**, 97-120.

Ashok K., H. Nakamura, and T. Yamagata, 2007: Impacts of ENSO and Indian Ocean dipole events on the Southern Hemisphere storm-track activity during austral winter. *Journal of Climate*, **20(13)**, 3147–3163.

Bengtsson L., K. I. Hodges,and E. Roeckner, 2006: Storm tracks and climate change. *Journal of Climate*, **19**, 3518-3543.

Bengtsson L., K. I. Hodges, and N. Keenlyside, 2009: Will extra-tropical storms intensify in a warmer climate? *Journal of Climate*, **22**, 2276–2301.

Bender F. A-M., V. Ramanathan, and G. Tselioudis, 2012: Changes in extratropical storm track cloudiness 1983-2008: Observation support for a poleward shift. *Climate Dynamics*, **38**, 2037-2053.

Blender R., K. Fraedrich, and F. Lunkeit, 1997: Identification of cyclone-track regimes in the North Atlantic. *Quarterly Journal of the Royal Meteorological Society*, **123**, 727-741.

Busuioc A. and H. von Storch, 1996: Changes in the winter precipitation in Romania and its relation to the large-scale circulation. *Tellus A*, **48**, 538 – 552.

Chang E. K. M., Y. Guo, and X. Xia, 2012: CMIP5 multimodel ensemble projection of storm track change under global warming, *Journal of Geophysical Research*, **117**, doi:10.1029/2012JD018578.

Chambers F. M., S. A. Brain, D. Mauquoy, J. McCarroll, and T. Daley. 2014: The ‘Little Ice Age’ in the Southern Hemisphere in the context of the last 3000 years: Peat-based proxy-climate date from Tierra del Fuego. *The Holocene*, **24**,1649-1656.

Chen F., H. von Storch, L. Zeng, Y. Du, 2014: Polar low genesis over the North Pacific under different global warming scenarios. *Climate Dynamics*, **43(12)**, 3449-3456.

Chu P., X. Zhao, J. Kim, 2010: Regional typhoon activity as revealed by track patterns and climate change. *Hurricanes and Climate Change*, **2**, 137-148.

Dierckx P., 1981: An algorithm for surface-fitting with spline functions. *IMA Journal of Numerical Analysis,* **1(3)**, 267-283.

Dierckx P., 1984: Algorithms for smoothing data on the sphere with tensor product splines. *Computing*, **32**, 319-342.

Eichler T. P. And J. Gottschalck 2013: A comparison of Southern Hemisphere cyclone track climatology and interannual variability in Coarse-Gridded Reanalysis Datasets. *Advances in Meteorology*, **2013**, doi:10.1155/2013/891260.

Elsner J. B., 2003: Tracking hurricanes. *Bulletin of the American Meteorological Society*, **84**, 353-356.

Fischer-Bruns I., H. von Storch, J. F. González-Rouco JF, and E. Zorita, 2005: Modelling the variablility of midlatitude storm activity on decadal to century time scales. *Climate Dynamics*, **25(5)**, 461-476.

González-Rouco F., H. von Storch, and E. Zorita, 2003: Deep soil temperature as proxy for surface air-temperature in a coupled model simulation of the last thousand years. *Geophysical Research Letters,* **30(21)**, L2116.

Gouirand I., V. Moron, E. Zorita, 2007: Teleconnections between ENSO and North Atlantic in an ECHO-G simulation of the 1000-1990 period. *Geophysical Research Letters,* **34**, L06705.

Goodwin I. D., S. Browning, A. M. Lorrey, P. A. Mayewski and et al., 2014: A reconstruction of extratropical Indo-Pacific sea-level pressure patterns during the Medieval Climate Anomaly. *Climate Dynamics*, **43**, 1197–1219.

Graff L. S. and J. H. Lacasce, 2012: Changes in the Extratropical Storm Tracks in Response to Changes in SST in an AGCM. *Journal of Climate*, **25**, 1854-1870.

Grise K. M., S.-W. Son, G. J. P. Correa, and L. M. Polvani, 2014: The response of extratropical cyclones in the Southern Hemisphere to stratospheric ozone depletion in the 20th century. *Atmospheric Science Letters*, **15(1)**, 29-36.

Hodges K. I., 1994: A general method for tracking analysis and its application to meteorological data. *Monthly Weather Review*, **122**, 2573-2586.

Hodges K. I., 1995: Feature tracking on the unit sphere. *Monthly Weather Review*,**123**, 3458-3465.

Hodges K. I., 1999: Adaptive constraints for feature tracking. *Monthly Weather Review*, **127**, 1362-1373.

Hoskins B. J. and K. I. Hodges, 2002: New perspectives on the Northern Hemisphere winter storm tracks. *Journal of the Atmospheric Sciences*, **59**, 1041-1061.

Hoskins B. J. and K. I. Hodges, 2005: A new perspective on Southern Hemisphere storm tracks. *Journal of Climate*, **18(20)**, 4108–4129.

Jung T., S. K. Gulev, I. Rudeva, V. Soloviov, 2006: Sensitivity of extratropical cyclone characteristic to horizontal resolution in ECMWF model. *Quarterly Journal of the Royal Meteorological Society*, **132**, 1839-1857.

Key J. R., and A. C. Chan, 1999: Multidecadal global and regional trends in 1000 mb and 500 mb cyclone frequencies. *Geophysical Research Letters*, **26**, 2053-2056.

Lim E. and I. Simmonds, 2007: Southern hemisphere winter extratropical cyclone characteristics and vertical organization observed with the ERA-40 data in 1979–2001. *Journal of Climate*, **20(11)**, 2675–2690.

Marsland S. J., M. Latif, and S. Legutke, 2003: Antarctic circumpolar modes in a coupled ocean–atmosphere model. *Ocean Dynamics*, **53(4)**, 323-331.

Matulla C., W. Schoener, H. Alexandersson, H. von Storch, XL Wang, 2008: European storminess: late nineteenth century to present. *Climate Dynamics*, **31**,125-130.

Meinardus, W., L. Mecking, 1928: Das Beobachtungsmaterial der internationalen meteorologischen Kooperation und seine Verwertung nebst Erläuterungen zum meteorologischen Atlas. -In: E.v. Drygalski (Hrsg.): Deutsche Südpolar-Expedition 1901-1903 im Auftrage des Reichsamtes des Innern. - Verlag Georg Reimer, Berlin, Bd. III: Meteorologie Band I, 2. Hälfte, Heft 1, 1-42.

Mendes D., E. P. Souza, J. A. Marengo, and M. C. D. Mendes, 2010: Climatology of extratropical cyclones over the South American-southern oceans sector. *Theoretical and Applied Climatology*, **100(3-4)**, 239–250.

Min S.-K.,S. Legutke, A. Hense, W.-T. Kwon, 2005a: Internal variability in a 1000-yr control simulation with the coupled climate model ECHO-G. I: near-surface temperature, precipitation and mean sea level pressure. *Tellus A*, **57**,605-621.

Min S.-K., S. Legutke S, A. Hense, W.-T. Kwon, 2005b: Internal variability in a 1000-yr control simulation with the coupled climate model ECHO-G. II: El Niño Southern Oscillation and North Atlantic Oscillation. *Tellus A*, **57**,622-640.

Murray R. J., and I. Simmonds, 1991: A numerical scheme for tracking cyclone centres from digital data Part I: development and operation of the scheme. *Australian Meteorological Magazine*, **39**, 155-166.

Nakamura J., U. Lall, Y. Kushnir, S. J. Camargo, 2009: Classifying North Atlantic tropical cyclone tracks by mass moments. *Journal of Climate*, **15**, 5481-5494.

Neukom R., J. Gergis, D. J. Karoly, H. Wanner and et al., 2014: Inter-hemispheric temperature variability over the past millennium. *Nature Climate Change*, doi: 10.1038/NCLIMATE2174.

Pezza A. B., I. Simmonds, J. A. Renwick, 2007: Southern Hemisphere cyclones and anticyclones: recent trends and links with decadal variability in the Pacific Ocean. *International Journal of Climatology*, **27**,1403-1419.

Pezza A. B., T. Durrant, I. Simmonds, and I. Smith, 2008: Southern hemisphere synoptic behavior in extreme phases of SAM, ENSO, sea ice extent, and Southern Australia rainfall. *Journal of Climate*, **21(21)**, 5566–5584.

Raible C. C. And R. Blender, 2004: Northern Hemisphere Mid-latitude cyclone variability in different ocean representations. *Climate Dynamics*, **22**, 239-248.

Rodgers K. B., P. Friederichs, and M. Latif, 2004: Tropical Pacific decadal variability and its relation to decadal modulations of ENSO. *Journal of Climate*, **17**, 3761-3774.

Roeckner E., K. Arpe, L. Bengtsson, M. Christoph, M. Claussen, L. Dümenil, M. Esch, M. Giorgetta, U. Schlese, U. Schulzweida, 1996: The atmopheric general circulation model ECHAM4: model description and simulation of present-day climate. Report No. 218, 90 pp, Max-Planck-Institut für Meteorologie, Bundesstr 55, Hamburg.

Rosenthal Y., B. K. Linsley and D. W. Oppo., 2013: Pacific Ocean heat content during the past 10,000 years. *Science*, **342**, 617-621.

Rudeva I., S. K. Gulev, 2007: Climatology of cyclone size characteristic and their changes during the cyclone life cycle. *Monthly Weather Review*, **135**, 2568-2587.

Serreze M. C., 1995: Climatological aspects of cyclone development and decay in the arctic. *Atmosphere-Ocean*, **33(1)**, 1-23.

Sickmöller M., R. Blender, and K. Fraedrich, 2000: Observed winter cyclone tracks in the northern hemisphere in re-analysed ECMWF data. *Quarterly Journal of the Royal Meteorological Society*, **126**, 591-620.

Simmonds I. and X. Wu, 1993: Cyclone behavior response to changes in winter Southern Hemisphere sea-ice concentration. *Quarterly Journal of the Royal Meteorological Society*, **119**, 1121-1148.

Simmonds I., and K. Keay, 2000a: Variability of Southern Hemisphere extratropical cyclone behavior, 1958–97. *Journal of Climate*, **13**, 550-561.

Simmonds I., and K. Keay, 2000b: Mean Southern Hemisphere extratropical cyclone behavior in the 40-year NCEP–NCAR reanalysis. *Journal of Climate*, **13**, 873-885.

Stendel M. And E. Roeckner, 1998: Impacts of horizontal resolution on simulated climate statistics in ECHAM4. Report No. 253, MaxPlanck-Institut für Meteorologie, Bundesstr 55, Hamburg.

Tan M., X. Shao, J. Liu, B. Cai, 2009: Comparative analysis between a proxy-based climate reconstruction and GCM-based simulation of temperature over the last millennium in China. *Journal of Quaternary Science*, **24(5)**, 547-551.

Ulbrich U., and M. Christoph, 1999: A shift of the NAO and increasing storm track activity over Europe due to anthropogenic greenhouse gas forcing. *Climate Dynamics*, **15**, 551-559.

van Loon, H., and J.J. Taljaard, 1962: Cyclogenesis, cyclones and anticyclones in the Southern Hemisphere during the winter and spring of 1957. *Notos*, **11**, 3–20.

van Loon, H., and J.J. Taljaard, 1963: Cyclogenesis, cyclones and anticyclones in the Southern Hemisphere during summer 1957–1958. *Notos*, **12**, 37–50.

von Storch H. And F. W. Zwiers, 1999: Statistical analysis in climate research. Cambridge University Press, Cambridge.

von Storch H., E. Zorita, Y. Dimitriev, F. González-Rouco, S. Tett, 2004: Reconstructing past climate from noisy data. *Science*, **306**, 679-682.

von Storch J.-S., V. Kharin, U. Cubasch, G. Hegerl, D. Schriever, H. von Storch, E. Zorita, 1997: A description of a 1260-year control integration with the coupled ECHAM1/LSG general circulation model. *Journal of Climate*, **10**, 1525-1543.

Vowinckel, E., and H. van Loon, 1957: Das Klima des Antarktischen Ozeans. *Archiv Meteor. Geophys. Bioklim.*, **B8**, 75– 102.

Wang, X. L. L., V. R. Swail, and F. W. Zwiers, 2004: Climatology and changes of extra-tropical storm tracks and cyclone activities as derived from two global reanalyses and the Canadian CGCM2 projections of future climate. In: Preprints of the eighth international workshop on wave forecast and hindcast, 14–19 November 2004, North Shore, Hawaii.

Wang, X. L. L., V. R. Swail, and F. W. Zwiers, 2006: Climatology and changes of extratropical cyclone activity: Comparison of ERA40 with NCEP–NCAR reanalysis for 1958–2001. *Journal of Climate*, **19**, 3145-3166.

Wernli H. and C. Schwierz, 2006: Surface cyclones in the ERA-40 dataset (1958–2001). Part I: novel identification method and global climatology. *Journal of the Atmospheric Sciences*, **63**, 2486-2507.

Wolff J. O., E. Maier-Reimer, S. Legutke, 1997: The Hamburg Ocean primitive equation model. Technical Report, No. 13, 98 pp, German Climate Computer Center (DKRZ), Hamburg.

Xia L., M. Zahn, K. I. Hodges, F. Feser, and H. von Storch, 2012: A comparison of two identification and tracking Methods for polar lows. *Tellus A*, **64**, 17196.

Xia L., H. von Storch, and F. Feser, 2013: Quasi-stationarity of centennial Northern Hemisphere midlatitude winter storm tracks. *Climate Dynamics*, **41**, 901-916.

Yin J. H., 2005: A consistent poleward shift of the storm tracks in simulations of the 21st century climate. *Geophysical Research Letters*, **32**, doi:10.1029/2005GL023684.

Zahn M. and H. von Storch, 2008a: Tracking polar lows in CLM. *Meteorologische Zeitschrift*, **17(4)**, 445–453.

Zahn M. and H. von Storch, 2008b: A long-term climatology of North Atlantic polar lows. *Geophysical Research Letters*,**35**, L22702.

Zolina O. and S. K. Gulev, 2002: Improving the accuracy of mapping cyclone numbers and frequencies. *Monthly Weather Review*, **130**, 748-759.

Zorita E., J. F. González-Rouco, H. von Storch, J. P. Montávez, and F. Valero, 2005: Natural and anthoropogenic model of surface temperature variations in the last thousand years. *Geophysical Research Letters*, **32**, L08707.

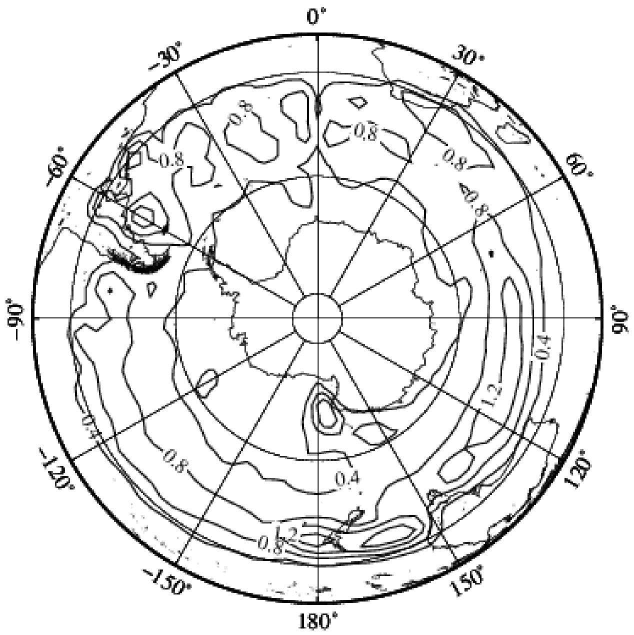

Fig. 1: 991-year (1000-1990) average density (unit: (3.75° *3.75°)$^{-1}$, about 110,000 km^{-2}) distribution of cyclone genesis in winter (JJA) for the Southern Hemisphere (SH) (Contour interval is 0.4/110,000 km^{2}).

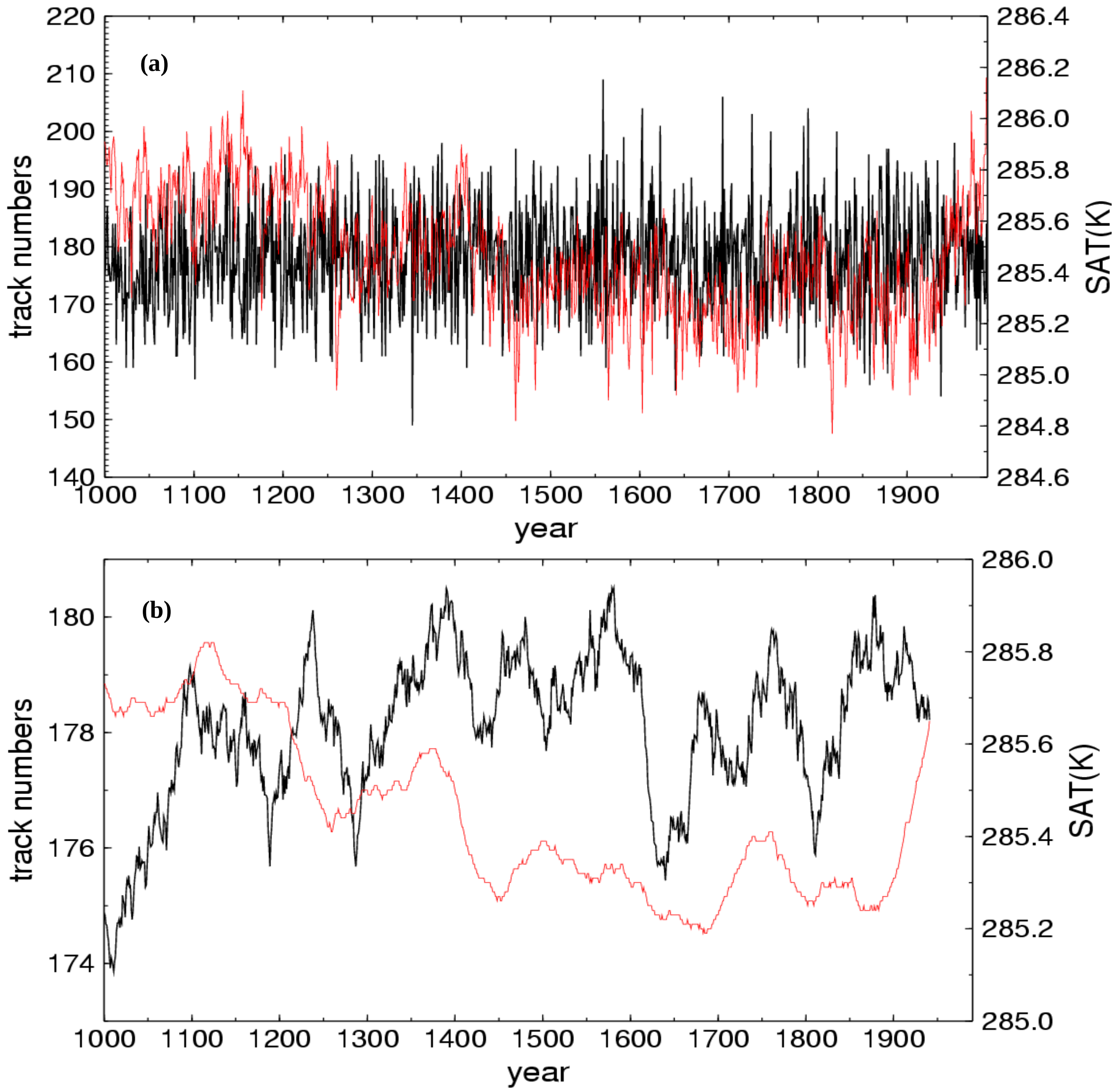

Fig. 2: (a): Time series of the numbers of winter (JJA) extratropical cyclones (black line) and winter surface air temperature (SAT: K) (red line) in the Southern Hemisphere (SH) (years 1000 – 1990); (b): same as (a) but for a smoothed time series by computing 50-year running means.

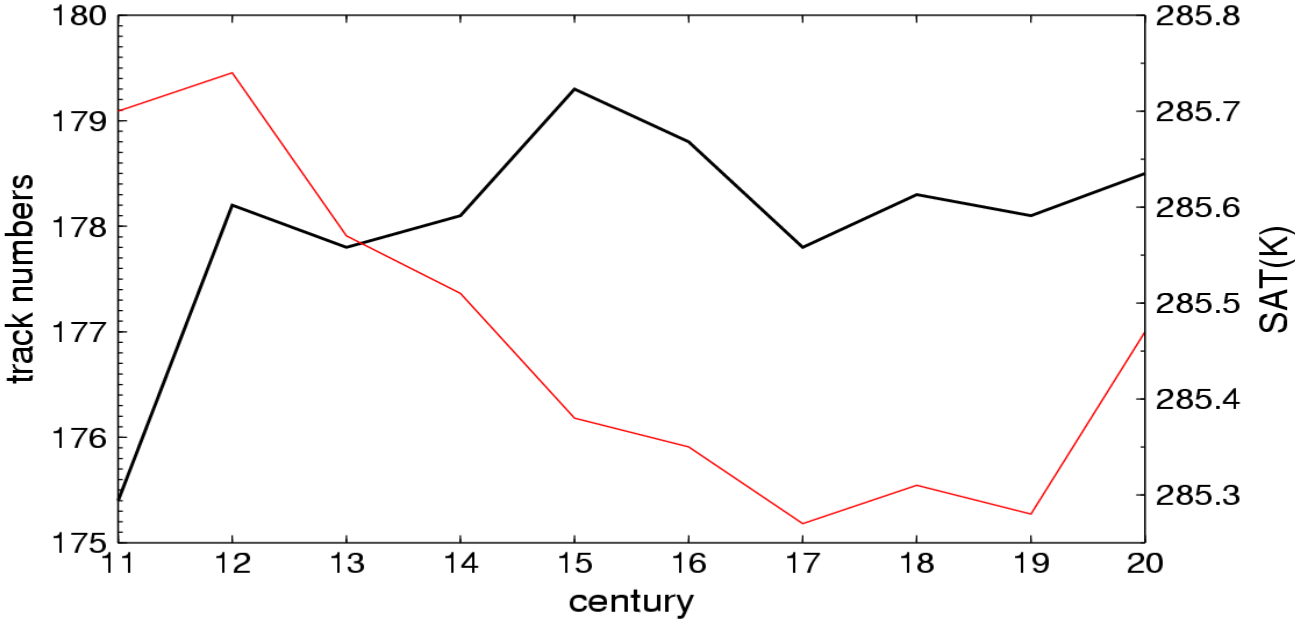

Fig. 3: Average annual numbers of winter (JJA) extratropical cyclones (black line) and average winter SAT (K) (red line) in the SH for different centuries (11th — 20th century).

Cluster 1

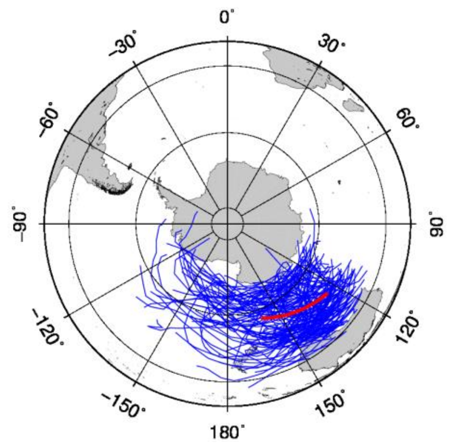

Cluster 2

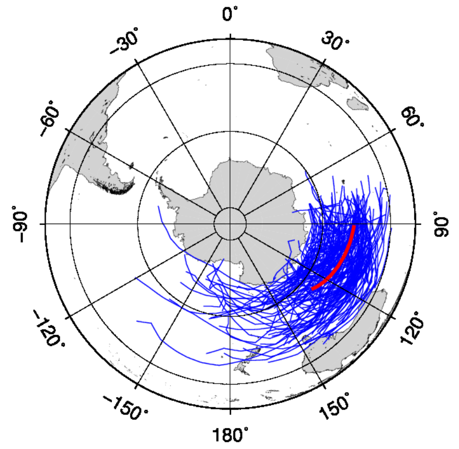

Cluster 3

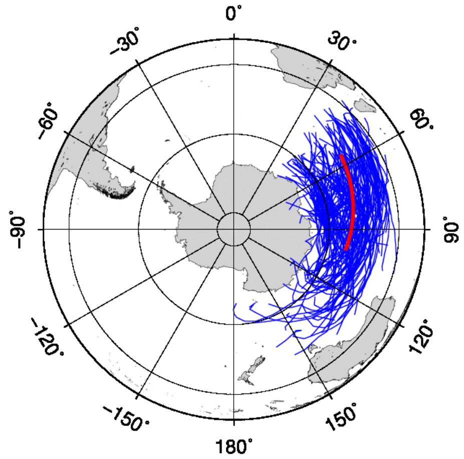

Cluster 4

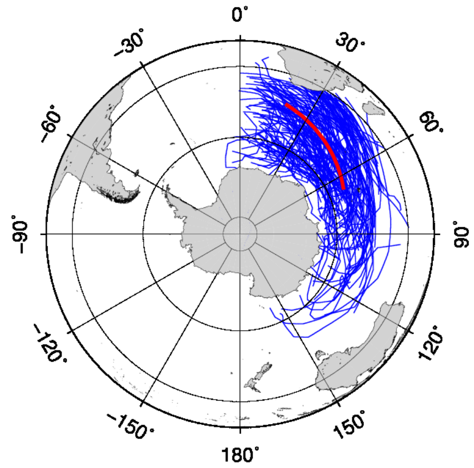

Cluster 5

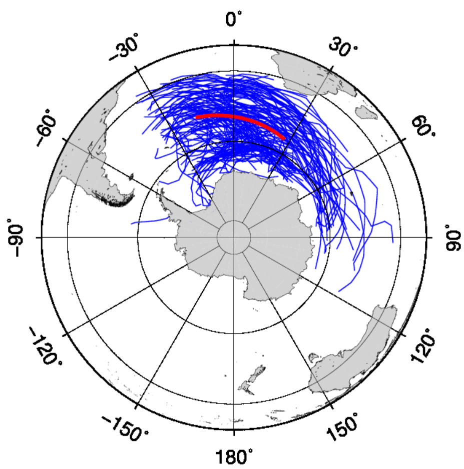

Cluster 6

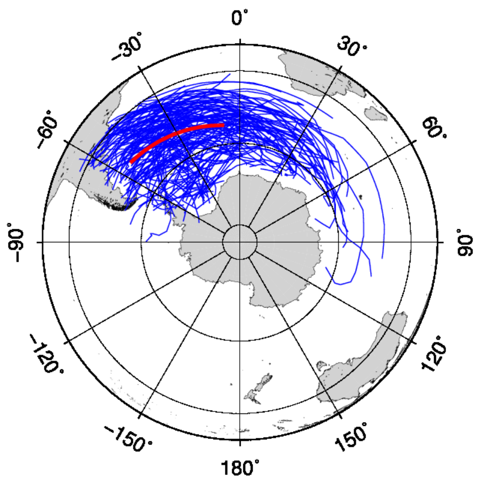

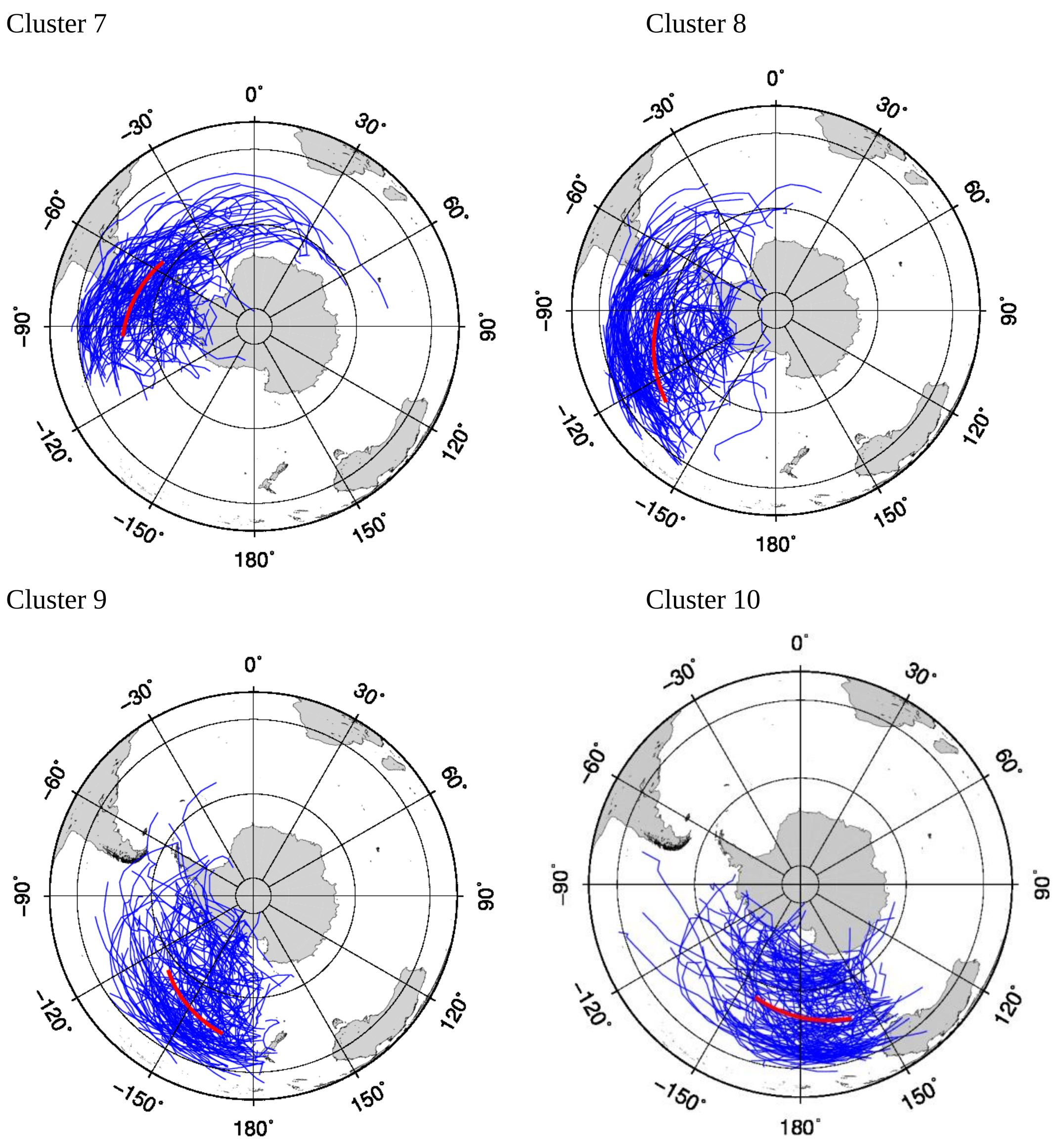

Fig. 4: Winter (JJA) extratropical cyclone tracks of the 20th century (years 1901-1990) in the SH clustered into ten clusters by applying the K-means method: member tracks (blue) and centroid tracks (red) of the ten clusters. Throughout the paper the ten clusters are grouped by ocean basins: Indian Ocean (cluster 1-4), South Atlantic (cluster 5-6) and South Pacific (cluster 7-10).

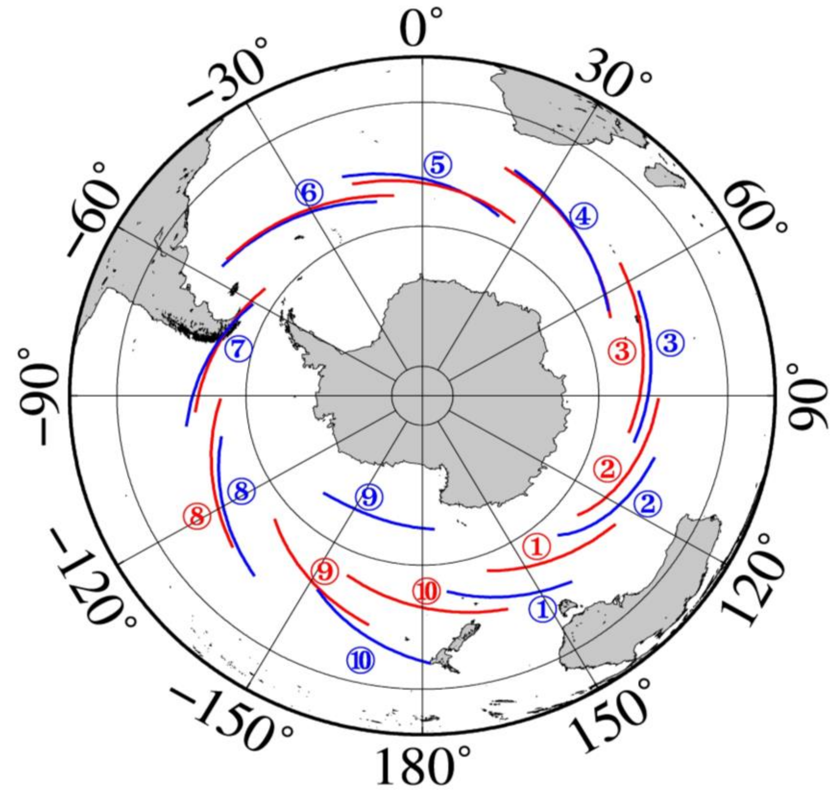

Fig. 5: Mean tracks of ten clusters for the SH in the 11th and 20th century: blue ones are the mean tracks of the ten clusters in the 11th century (years 1000-1099), red ones are the mean tracks of the ten clusters in the 20th century (years 1900-1990).

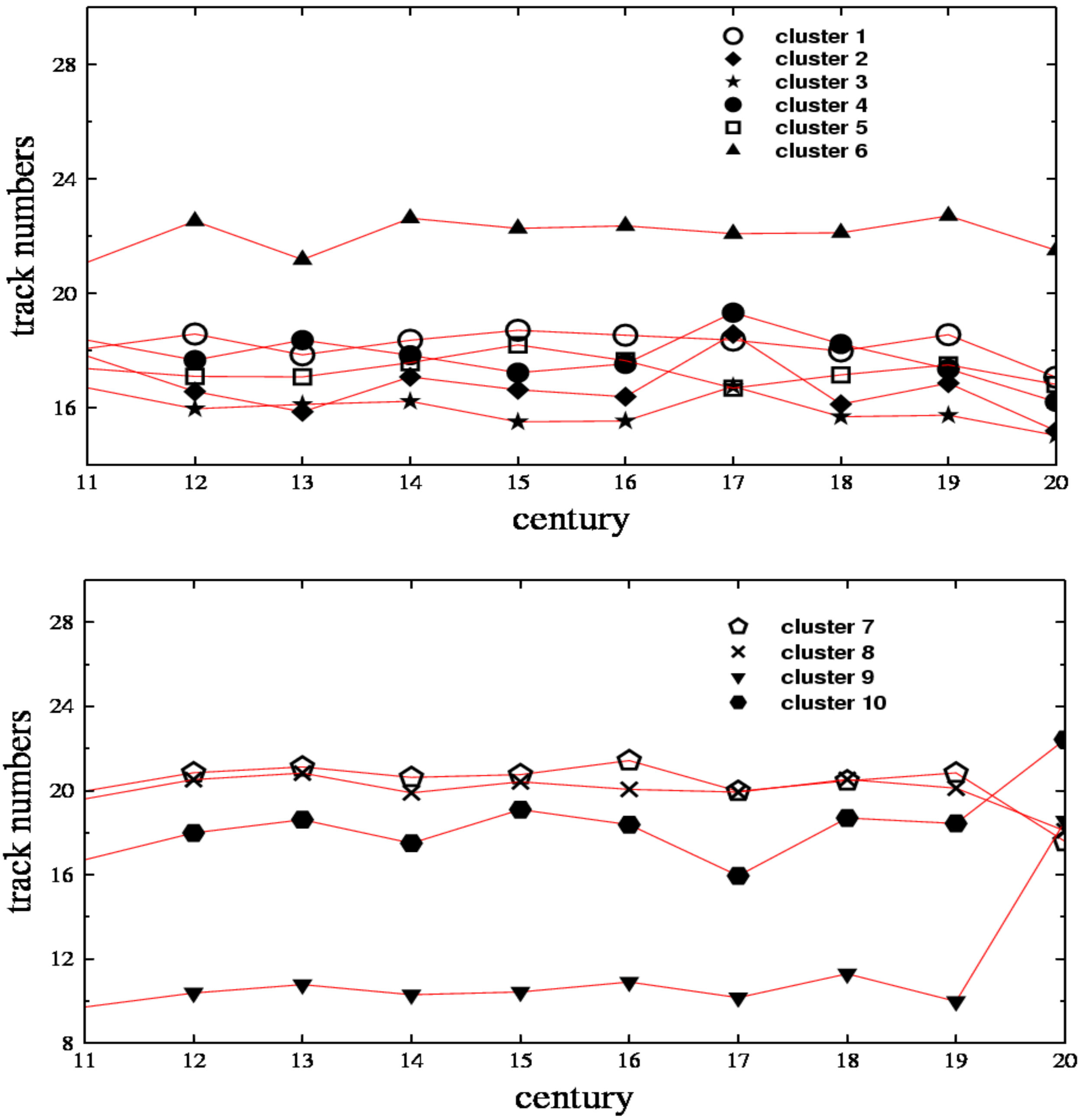

Fig.6: Average annual numbers of winter (JJA) extratropical cyclones in the SH for the ten clusters in different centuries (11th -20th century): top panel for the Indian Ocean (cluster 1-4) and the South Atlantic (cluster 5-6); bottom panel for the South Pacific (cluster 7-10).

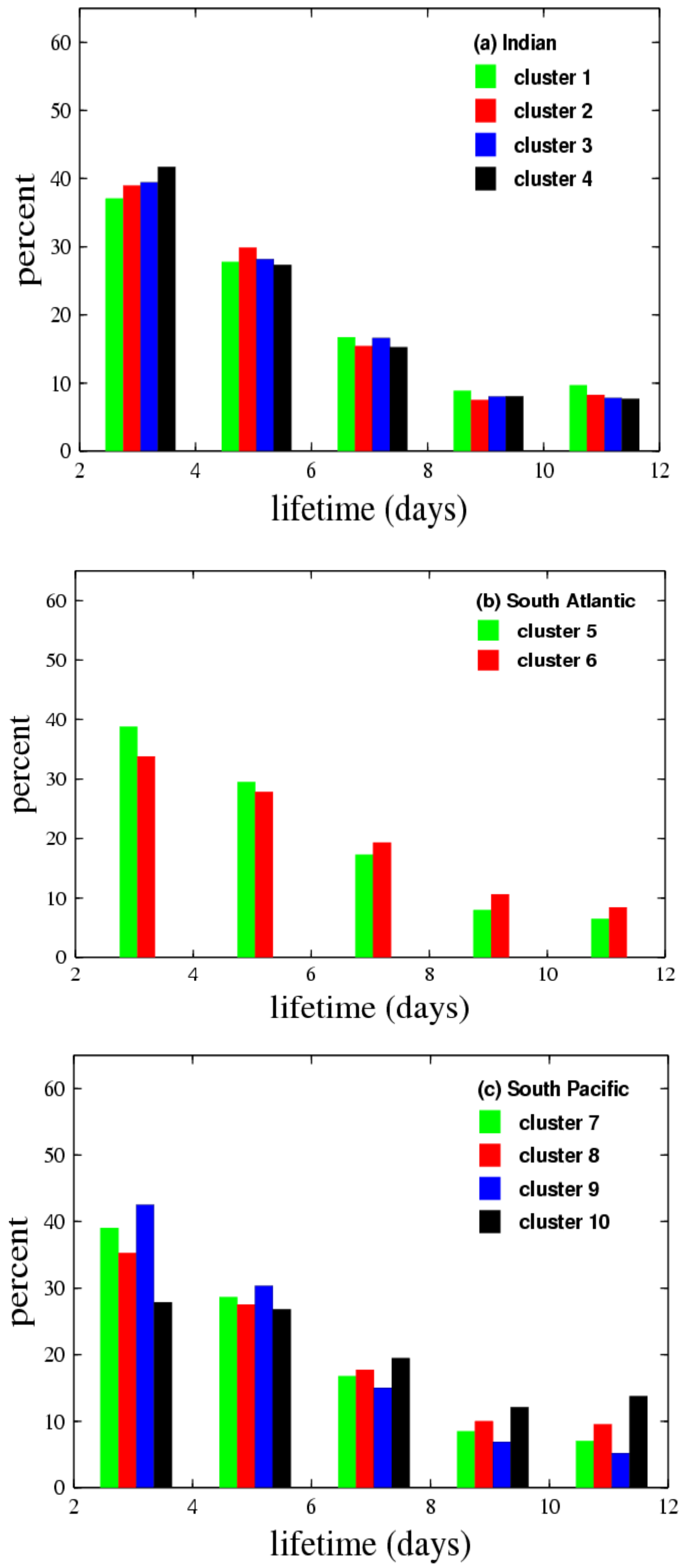

Fig. 7: Distributions (%) of cyclone lifetime (days) for winter cyclones over the Indian Ocean (a), the South Atlantic (b) and the South Pacific (c) for the whole time period (year 1000-1990).

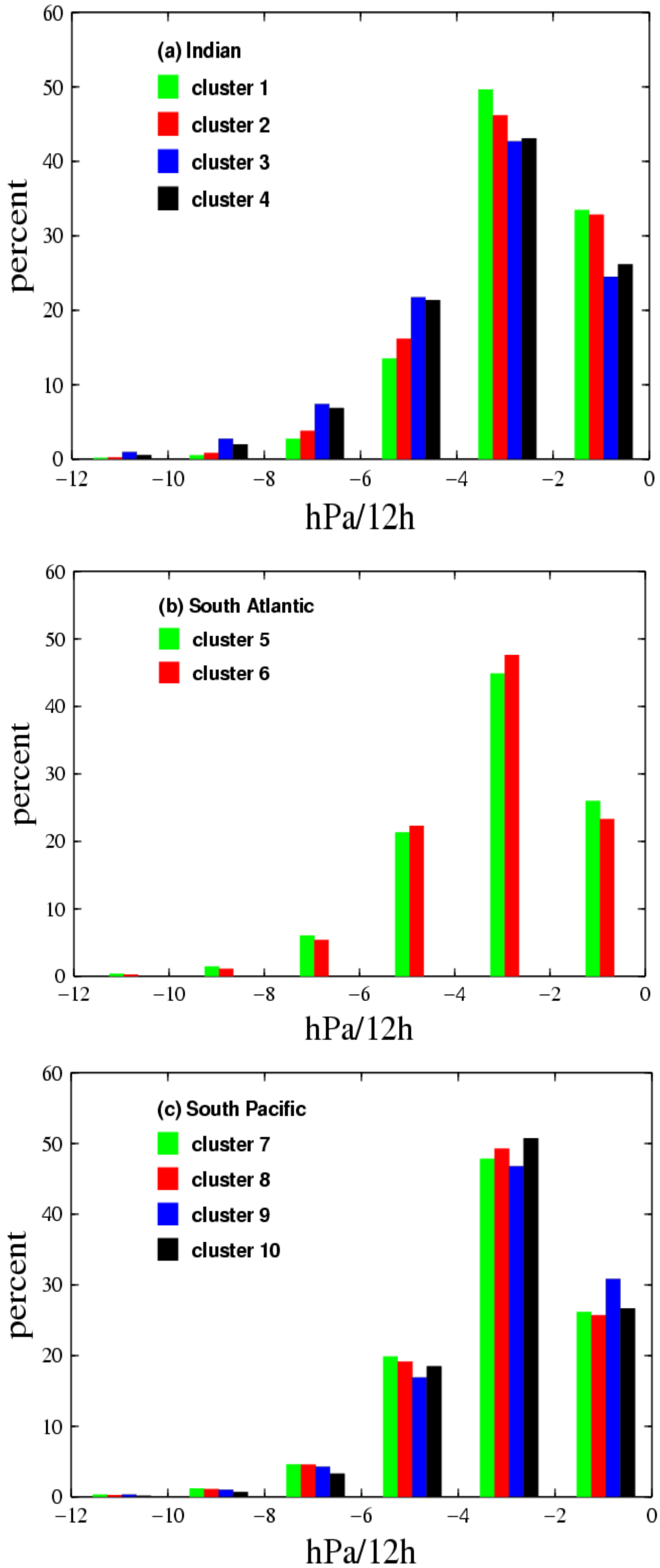

Fig. 8: Distributions (%) of cyclone mean deepening rates (hPa/12 h) for winter cyclones over the Indian Ocean (a), the South Atlantic (b) and the South Pacific (c) for the whole time period (year 1000-1990).

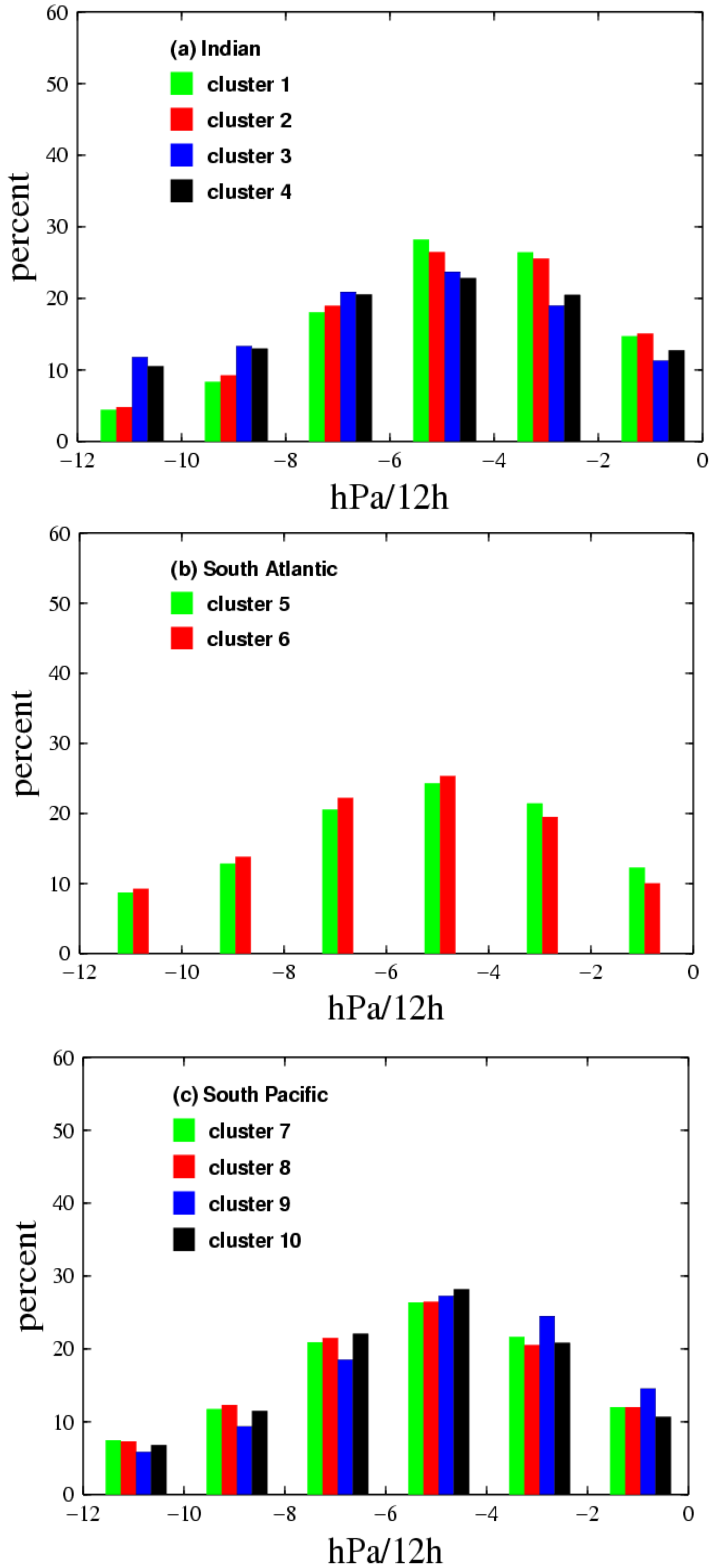

Fig. 9: Distributions (%) of cyclone maximum deepening rates (hPa/12 h) for winter cyclones over the Indian Ocean (a), the South Atlantic (b) and the South Pacific (c) for the whole time period (year 1000-1990).

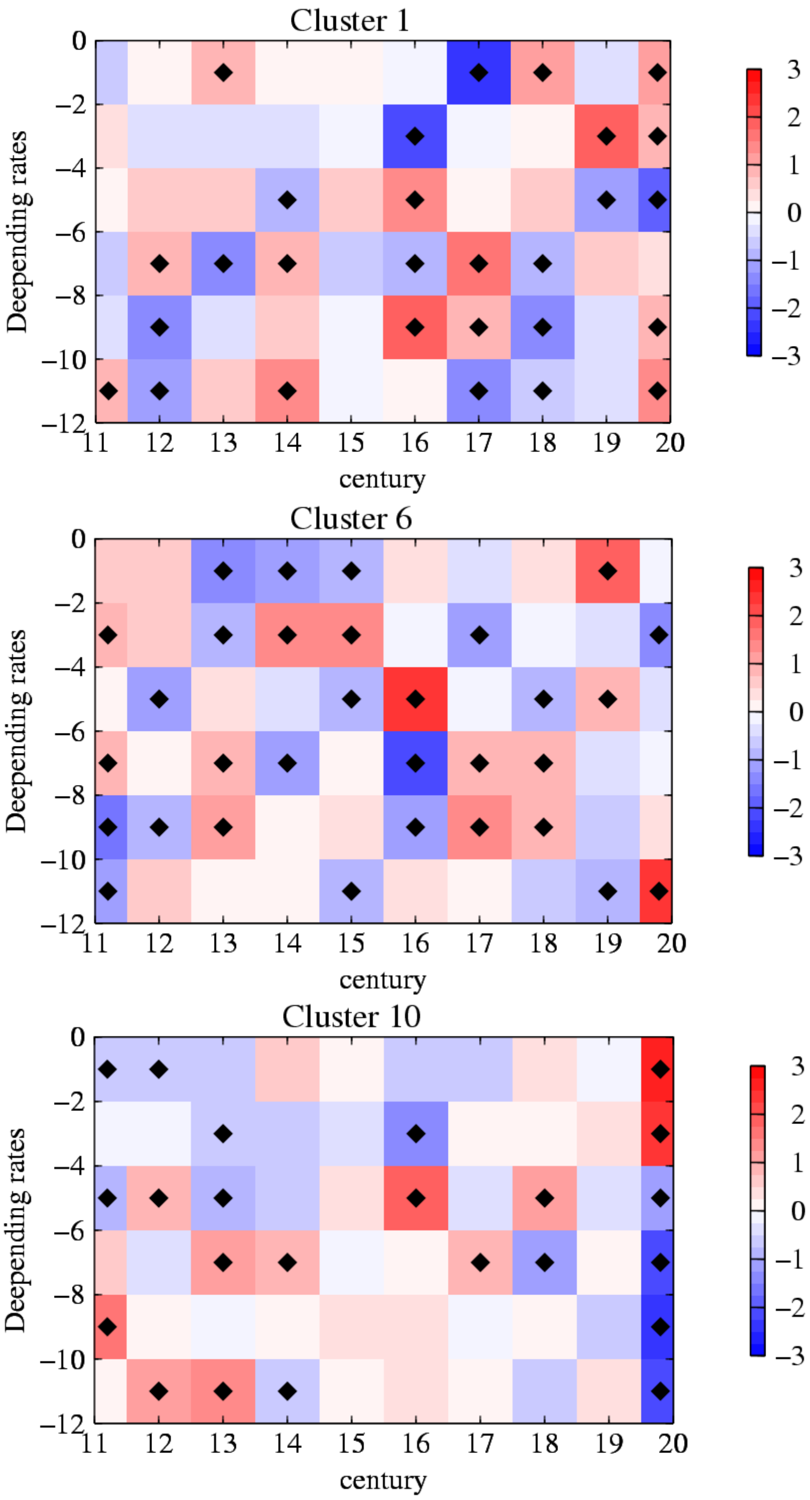

Fig. 10: Normalized anomalies of the cyclone maximum deepening rates (hPa/12 h) distributions for cluster members over the Indian Ocean (cluster 1), the South Atlantic (cluster 6) and the South Pacific (cluster 10) across different centuries (11^{th} —20^{th} century): the diamond symbol indicates that the anomaly is significant according to a t-test at the 95% level.

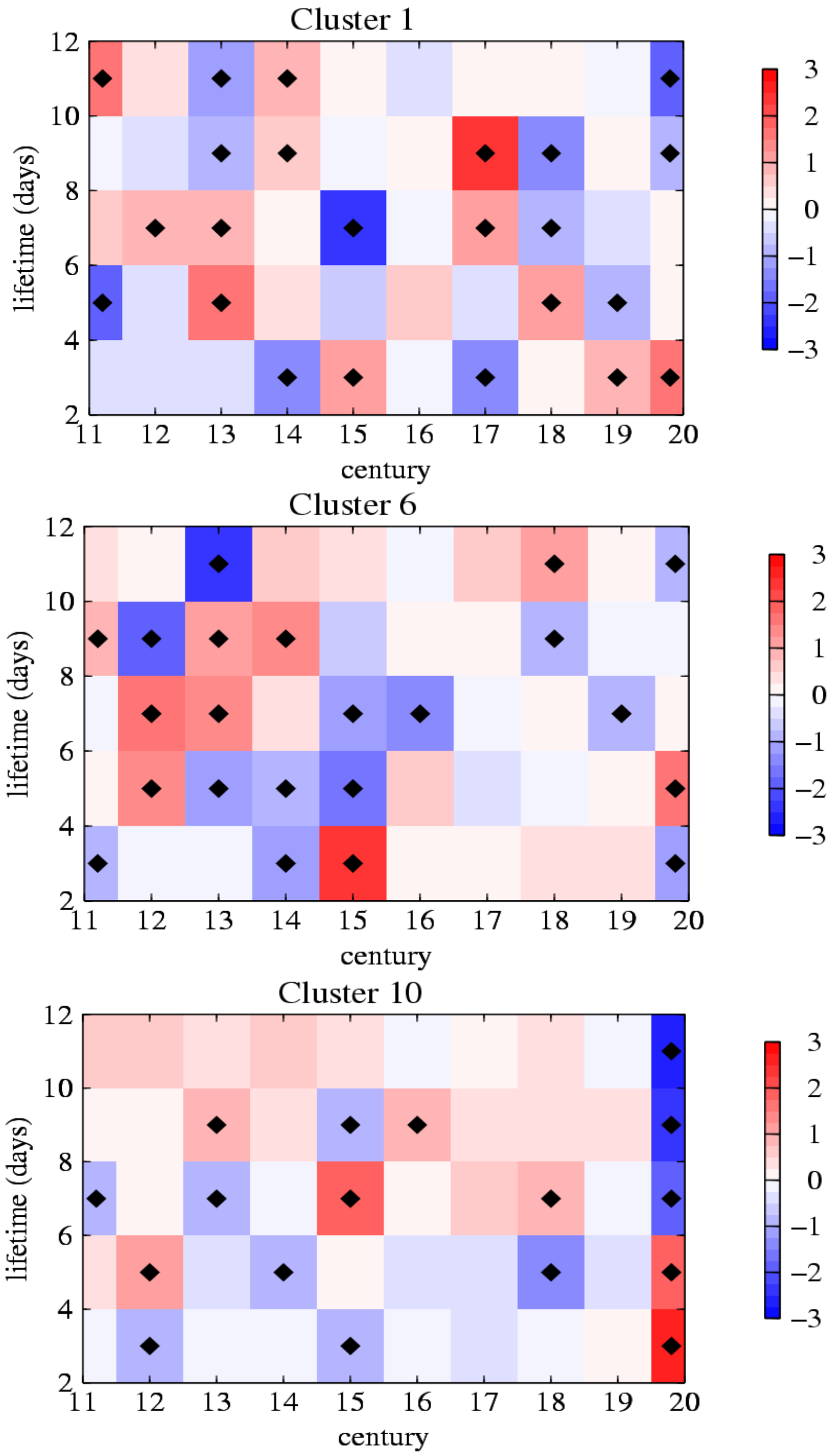

Fig. 11: Normalized anomalies of the cyclone lifetime (days) distributions for cluster members over the Indian Ocean (cluster 1), the South Atlantic (cluster 6) and the South Pacific (cluster 10) across different centuries (11th —20th century): the diamond symbol indicates that the anomaly is significant according to a t-test at the 95% level.

.

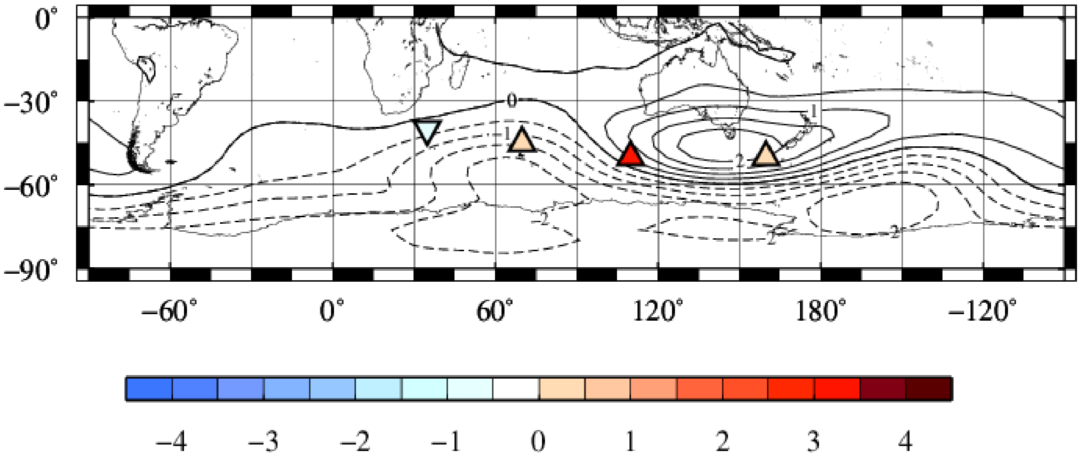

Fig. 16: Corresponding correlation patterns between time series of winter (JJA) cyclone numbers in the Indian Ocean (cluster 1, 2, 3 and 4) (symbols represent the mean centroid position of each cluster over the whole period: triangles for positive values, inverted triangles for negative values) and mean sea level pressure fields in hPa (isolines: dashed for negative and solid for positive; contour interval is 0.5 hPa). The first CCA pair shares a correlation coefficient of 0.42 and represents 25% of the variance of winter cyclone numbers from year 1000 to 1990. Cyclone frequency anomalies are 0.45 for cluster 1, 3.41 for cluster 2, 0.25 for cluster 3, but -1.14 for cluster 4.

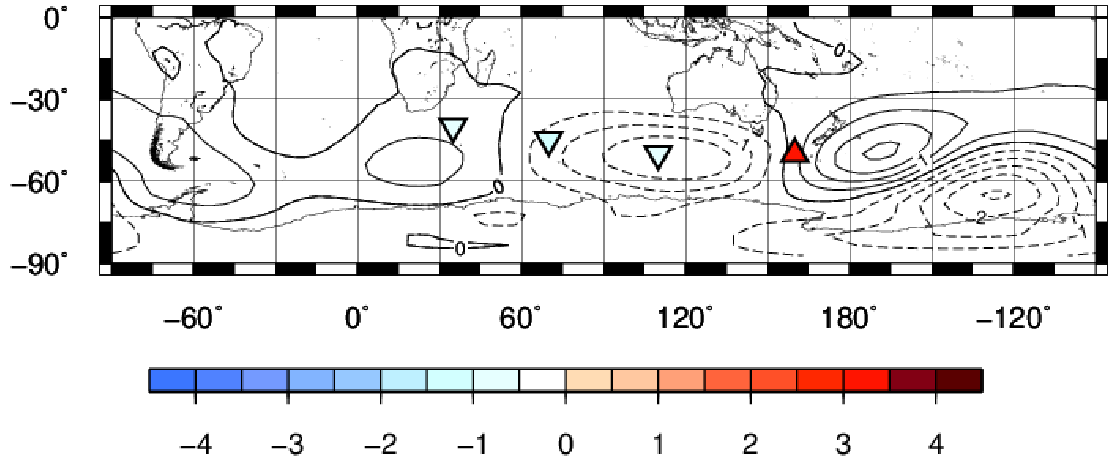

Fig. 17: Same as Fig. 16 for the second CCA pair: it shares a correlation coefficient of 0.33 and represents 25% of the variance of winter cyclone numbers from year 1000 to 1990. Cyclone frequency anomalies are 3.27 for cluster 1, but -0.73 for cluster 2, -1.31 for cluster 3, -0.62 for cluster 4.

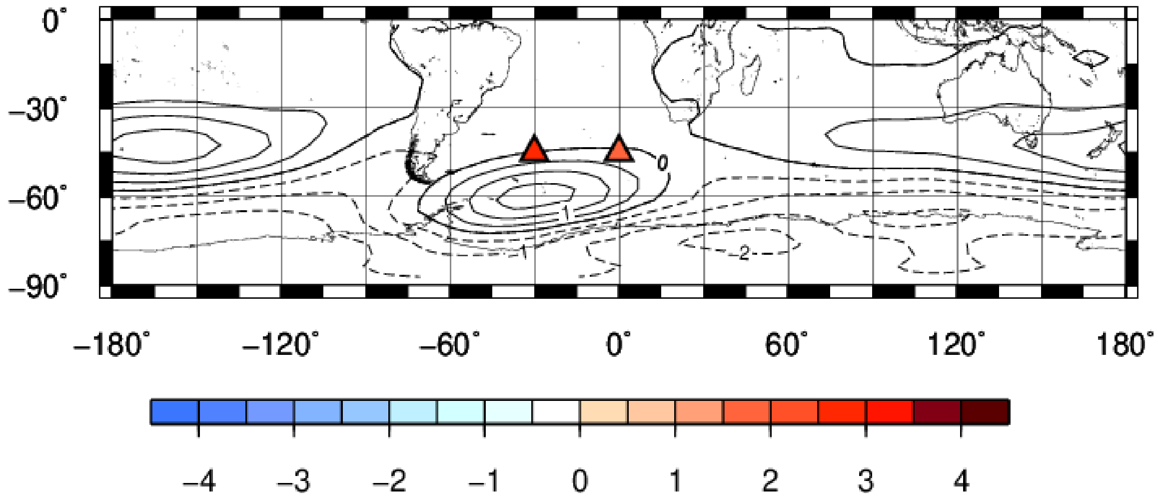

Fig. 18: Corresponding correlation patterns between time series of winter (JJA) cyclone numbers in the South Atlantic (cluster 5 and 6) (symbols represent the mean centroid position of each cluster over the whole period: triangles for positive values, inverted triangles for negative values) and mean sea level pressure fields in hPa (isolines: dashed for negative and solid for positive; contour interval is 0.5 hPa). The first CCA pair shares a correlation coefficient of 0.29 and represents 42% of the variance of winter cyclone numbers from year 1000 to 1990. Cyclone frequency anomalies are 1.91 for cluster 5 and 2.91 for cluster 6.

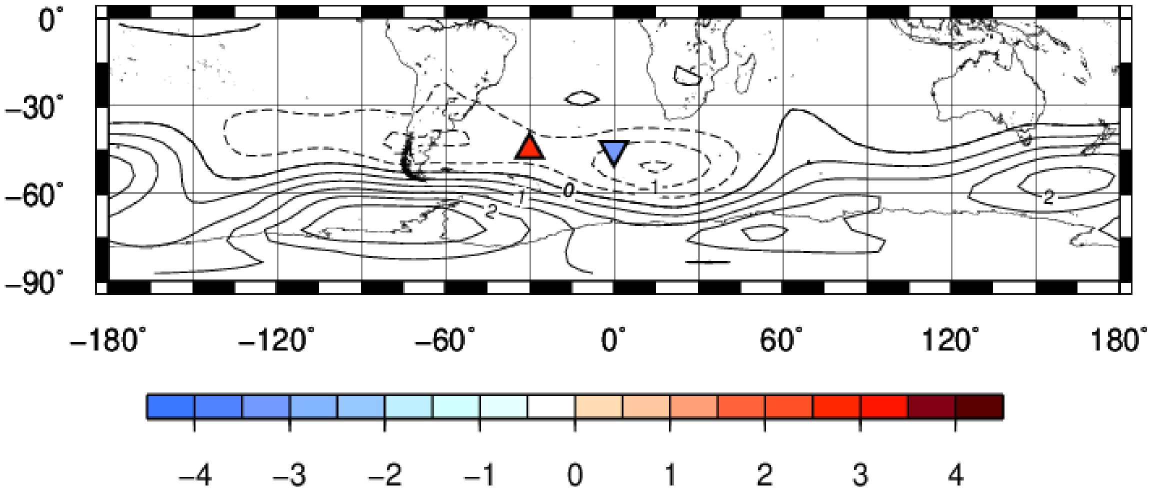

Fig. 19: Same as Fig. 18 for the second CCA pair: it shares a correlation coefficient of 0.17 and represents 58% of the variance of winter cyclone numbers from year 1000 to 1990. Cyclone frequency anomalies are -3.14 for cluster 5, but 2.58 for cluster 6.

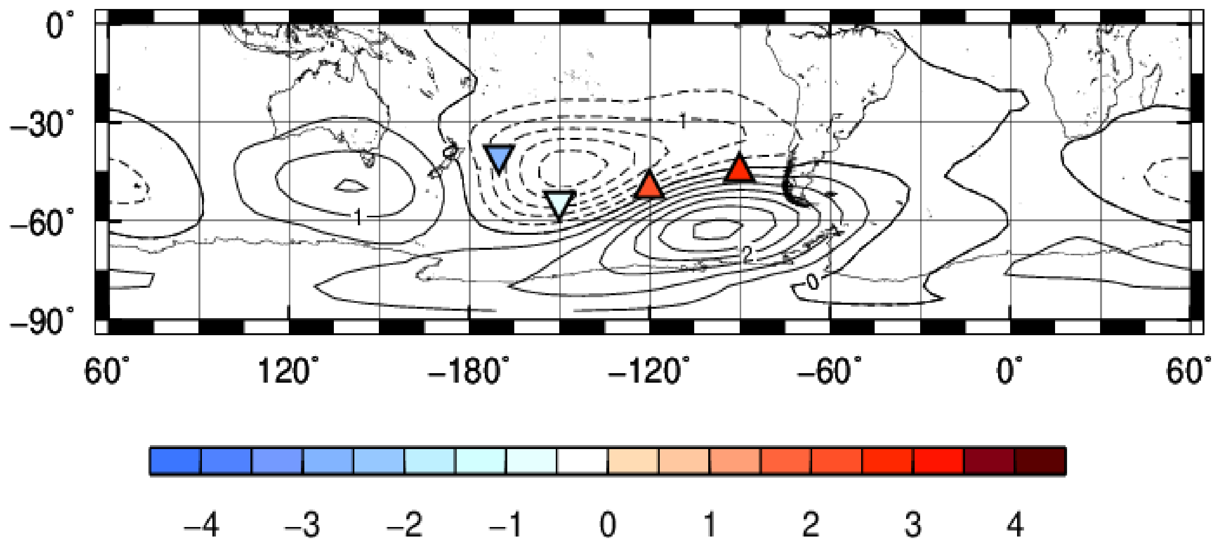

Fig. 20: Corresponding correlation patterns between time series of winter (JJA) cyclone numbers in the South Pacific (cluster 7, 8, 9 and 10) (symbols represent the mean centroid position of each cluster over the whole period: triangles for positive values, inverted triangles for negative values) and mean sea level pressure fields in hPa (isolines: dashed for negative and solid for positive; contour interval is 0.5 hPa). The first CCA pair shares a correlation coefficient of 0.44 and represents 31% of the variance of winter cyclone numbers from year 1000 to 1990. Cyclone frequency anomalies are 2.70 for cluster 7, 2.17 for cluster 8, -0.55 for cluster 9 and -2.64 for cluster 10.

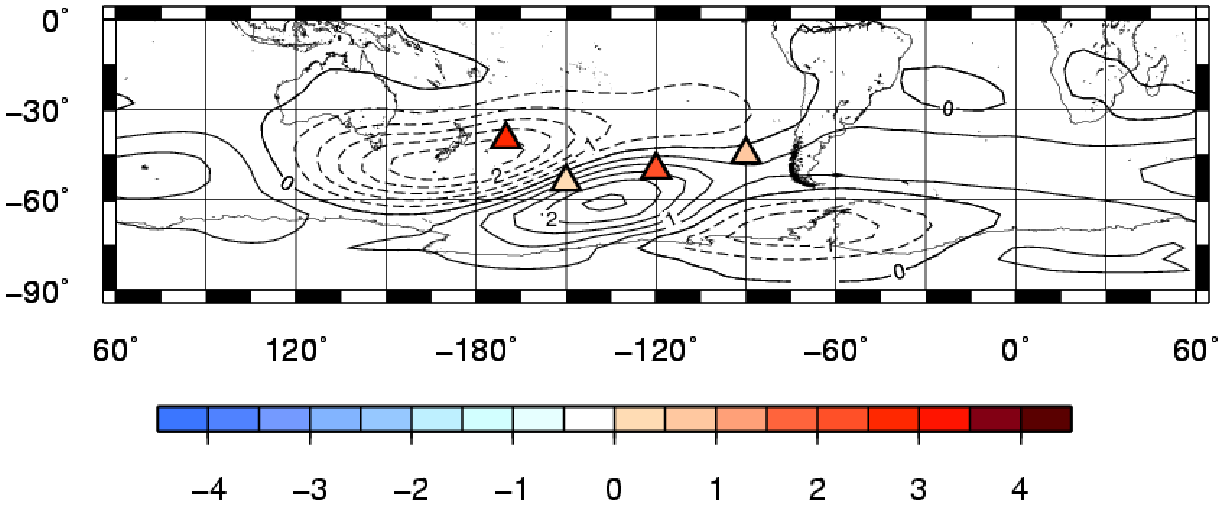

Fig. 21: Same as Fig. 20 for the second CCA pair: it shares a correlation coefficient of 0.42 and represents 19% of the variance of winter cyclone numbers from year 1000 to 1990. Cyclone frequency anomalies are 0.73 for cluster 7, 2.01 for cluster 8, 0.24 for cluster 9, and 2.76 for cluster 10.

Table 1: Cyclone numbers of the ten clusters shown in Fig. 4 for the quasi-millennial time period (years 1000-1990).

Cluster	1	2	3	4	5	6	7	8	9	10
Numbers	18057	16574	15794	17669	17163	21855	20206	19837	11082	18180

Table 2: Lifespan (day) distribution rates (numbers in bold) of the ten clusters for the quasi-millennial time period (years 1000-1990); numbers in brackets are normalized between different clusters for each distribution. (Unit :%)

Lifetime(days)	[2, 4)	[4, 6)	[6, 8)	[8, 10)	≥10
Cluster 1	**37.06** (10.22)	**27.77** (10.05)	**16.70** (9.99)	**8.84** (10.06)	**9.63** (11.57)
Cluster 2	**38.98** (9.87)	**29.86** (9.92)	**15.41** (8.46)	**7.50** (7.83)	**8.25** (9.11)
Cluster 3	**39.42** (9.51)	**28.19** (8.93)	**16.61** (8.69)	**8.01** (7.97)	**7.77** (8.17)
Cluster 4	**41.73** (11.26)	**27.33** (9.68)	**15.25** (8.93)	**8.05** (8.97)	**7.64** (8.99)
Cluster 5	**38.79** (10.17)	**29.49** (10.15)	**17.29** (9.84)	**7.95** (8.60)	**6.47** (7.39)
Cluster 6	**33.80** (11.28)	**27.85** (12.20)	**19.32** (13.99)	**10.61** (14.61)	**8.42** (12.25)
Cluster 7	**39.06** (12.05)	**28.64** (11.60)	**16.77** (11.23)	**8.48** (10.80)	**7.05** (9.48)
Cluster 8	**35.28** (10.69)	**27.54** (10.95)	**17.70** (11.64)	**9.96** (12.45)	**9.52** (12.57)
Cluster 9	**42.56** (7.20)	**30.35** (6.74)	**15.00** (5.51)	**6.89** (4.81)	**5.21** (3.84)
Cluster 10	**27.88** (7.74)	**26.81** (9.77)	**19.45** (11.72)	**12.11** (13.88)	**13.75** (16.64)

Table 3: Mean deepening rate (hPa/12h) distributions (numbers in bold) of the ten clusters for the quasi-millennial time period (years 1000-1990); numbers in brackets are normalized between different clusters for each distribution. (Unit :%)

Mean deepending rates (hPa/12h)	<-10	[-10, -8)	[-8, -6)	[-6, -4)	[-4, -2)	[-2, 0)
Cluster 1	**0.14** (4.02)	**0.53** (4.31)	**2.72** (5.59)	**13.50** (7.10)	**49.66** (10.70)	**33.44** (12.39)
Cluster 2	**0.26** (6.70)	**0.82** (6.11)	**3.77** (7.13)	**16.18** (7.80)	**46.17** (9.11)	**32.80** (11.21)
Cluster 3	**0.96** (24.29)	**2.73** (19.55)	**7.41** (13.59)	**21.73** (10.16)	**42.66** (8.17)	**24.51** (8.08)
Cluster 4	**0.54** (15.41)	**1.99** (15.95)	**6.85** (14.01)	**21.35** (11.09)	**43.08** (9.16)	**26.18** (9.60)
Cluster 5	**0.39** (10.72)	**1.44** (11.17)	**6.04** (12.05)	**21.33** (10.77)	**44.83** (9.27)	**25.97** (9.24)
Cluster 6	**0.27** (9.38)	**1.11** (11.17)	**5.41** (13.88)	**22.31** (14.52)	**47.63** (12.69)	**23.27** (10.69)
Cluster 7	**0.33** (10.72)	**1.21** (11.12)	**4.62** (10.81)	**19.86** (11.83)	**47.80** (11.65)	**26.18** (10.99)
Cluster 8	**0.28** (8.71)	**1.08** (9.70)	**4.57** (10.50)	**19.14** (11.21)	**49.24** (11.79)	**25.70** (10.60)
Cluster 9	**0.29** (5.53)	**1.01** (5.06)	**4.26** (5.46)	**16.88** (5.50)	**46.74** (6.19)	**30.82** (6.97)
Cluster 10	**0.15** (4.52)	**0.71** (5.87)	**3.27** (6.99)	**18.48** (10.03)	**50.73** (11.27)	**26.67** (10.22)

Table 4: Maximum deepening rate (hPa/12h) distributions (numbers in bold) of the ten clusters for the quasi-millennial time period (years 1000-1990); numbers in brackets are normalized between different clusters for each distribution. (Unit :%)

Maximum deepending rates (hPa/12h)	<-10	[-10, -8)	[-8, -6)	[-6, -4)	[-4, -2)	[-2, 0)
Cluster 1	**4.39** (5.73)	**8.30** (7.20)	**18.04** (8.87)	**28.20** (11.03)	**26.39** (12.24)	**14.70** (12.02)
Cluster 2	**4.81** (5.71)	**9.19** (7.30)	**18.95** (8.55)	**26.44** (9.47)	**25.56** (10.92)	**15.07** (11.38)
Cluster 3	**11.81** (13.66)	**13.31** (10.27)	**20.91** (9.15)	**23.71** (8.24)	**18.98** (7.84)	**11.28** (8.21)
Cluster 4	**10.52** (13.56)	**12.95** (11.10)	**20.54** (9.99)	**22.83** (8.81)	**20.45** (9.37)	**12.72** (10.31)
Cluster 5	**8.69** (10.92)	**12.79** (10.66)	**20.56** (9.71)	**24.31** (9.13)	**21.41** (9.55)	**12.24** (9.61)
Cluster 6	**9.23** (14.91)	**13.77** (14.81)	**22.19** (13.50)	**25.33** (12.25)	**19.49** (11.22)	**9.99** (10.13)
Cluster 7	**7.44** (10.97)	**11.70** (11.47)	**20.91** (11.66)	**26.34** (11.66)	**21.65** (11.38)	**11.97** (11.08)
Cluster 8	**7.29** (10.58)	**12.29** (11.87)	**21.50** (11.77)	**26.45** (11.50)	**20.49** (10.57)	**11.99** (10.91)
Cluster 9	**5.86** (4.79)	**9.36** (5.04)	**18.50** (5.63)	**27.27** (6.55)	**24.48** (6.92)	**14.53** (7.28)
Cluster 10	**6.80** (9.17)	**11.47** (10.28)	**22.05** (11.18)	**28.18** (11.36)	**20.82** (9.99)	**10.68** (9.06)